Cell Reports

Article

# Structural Basis for Regulation of the Opposing (p)ppGpp Synthetase and Hydrolase within the Stringent Response Orchestrator Rel

## Graphical Abstract

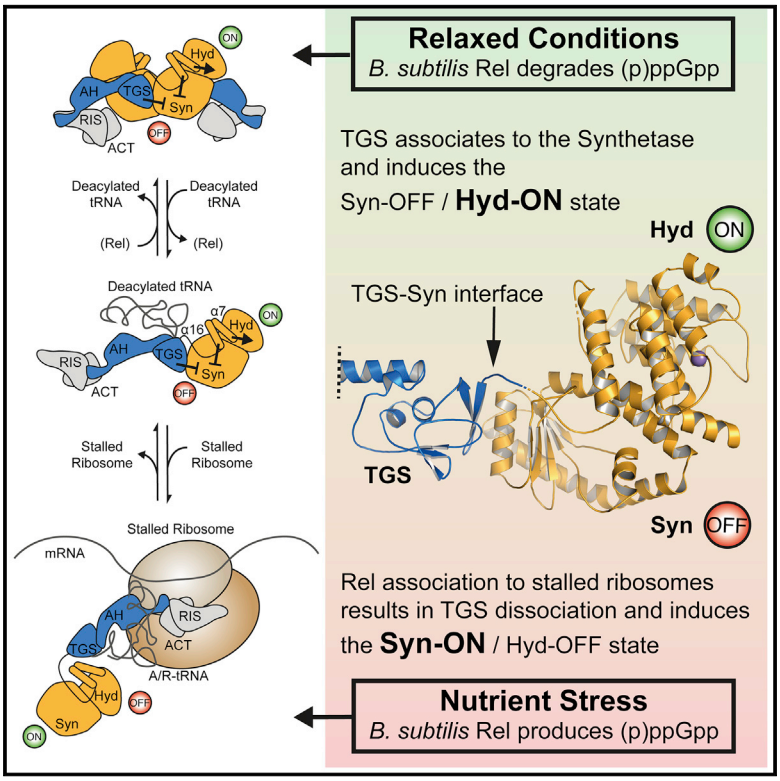


## Authors

Patrick Pausch, Maha Abdelshahid, Wieland Steinchen, ..., Kürşad Turgay, Daniel N. Wilson, Gert Bange

## Correspondence

turgay@mpusp.mpg.de (K.T.), daniel.wilson@chemie.uni-hamburg.de (D.N.W.), gert.bange@synmikro.uni-marburg.de (G.B.)

## In Brief

Pausch et al. report the structural and functional analysis of the bifunctional regulator of the (p)ppGpp-dependent stringent response in its free and ribosome-bound state. The study provides a detailed molecular view into the bacterial mechanism of stringent response repression in the absence of stress.

## Highlights

- Crystal structure of apo *B. subtilis* Rel
- Cryo-EM structure of the Rel•stalled ribosome complex
- Rel is regulated by the TGS domain in absence of the ribosome
- Rel homodimerization masks the tRNA interaction interface

Pausch et al., 2020, Cell Reports *32*, 108157
September 15, 2020 
https://doi.org/10.1016/j.celrep.2020.108157

CellPress

Cell Reports

CellPress
OPEN ACCESS

Article

# Structural Basis for Regulation of the Opposing (p)ppGpp Synthetase and Hydrolase within the Stringent Response Orchestrator Rel

Patrick Pausch,[1,6] Maha Abdelshahid,[2] Wieland Steinchen,[1] Heinrich Schäfer,[3] Fabio Lino Gratani,[4] Sven-Andreas Freibert,[5] Christiane Wolz,[4] Kürşad Turgay,[3,*] Daniel N. Wilson,[2,*] and Gert Bange[1,7,*]

[1]Center for Synthetic Microbiology & Department of Chemistry, Hans-Meerwein-Strasse, C07, Philipps-University Marburg, 35043 Marburg, Germany

[2]Institute for Biochemistry and Molecular Biology, University of Hamburg, 20146 Hamburg, Germany

[3]Leibniz University of Hannover, Institute for Microbiology & Max Planck Unit for the Science of Pathogens, Charitéplatz 1, 10117 Berlin, Germany

[4]Interfaculty Institute of Microbiology and Infection Medicine, University of Tübingen, 72076 Tübingen, Germany

[5]Center for Synthetic Microbiology & Institute for Cytobiology and Cytopathology, Philipps-University Marburg, 35043 Marburg, Germany

[6]Present address: Innovative Genomics Institute, University of California, Berkeley, 2151 Berkeley Way, Berkeley, CA 94720, USA

[7]Lead Contact

*Correspondence: turgay@mpusp.mpg.de (K.T.), daniel.wilson@chemie.uni-hamburg.de (D.N.W.), gert.bange@synmikro.uni-marburg.de (G.B.)

https://doi.org/10.1016/j.celrep.2020.108157

## SUMMARY

The stringent response enables metabolic adaptation of bacteria under stress conditions and is governed by RelA/SpoT Homolog (RSH)-type enzymes. Long RSH-type enzymes encompass an N-terminal domain (NTD) harboring the second messenger nucleotide (p)ppGpp hydrolase and synthetase activity and a stress-perceiving and regulatory C-terminal domain (CTD). CTD-mediated binding of Rel to stalled ribosomes boosts (p)ppGpp synthesis. However, how the opposing activities of the NTD are controlled in the absence of stress was poorly understood. Here, we demonstrate on the RSH-type protein Rel that the critical regulative elements reside within the TGS (ThrRS, GTPase, and SpoT) subdomain of the CTD, which associates to and represses the synthetase to concomitantly allow for activation of the hydrolase. Furthermore, we show that Rel forms homodimers, which appear to control the interaction with deacylated-tRNA, but not the enzymatic activity of Rel. Collectively, our study provides a detailed molecular view into the mechanism of stringent response repression in the absence of stress.

## INTRODUCTION

Metabolic adaptation upon alteration of environmental conditions, emerging cellular stress, and nutrient limitation is essential for the fitness of living organisms. Most bacteria and the chloroplasts of plants use the stringent response (SR) to adjust transcription, translation, and metabolic pathways for control over growth and cell proliferation, but also pathogenicity (summarized in Hauryliuk et al., 2015; Steinchen and Bange, 2016). At the heart of the SR, RelA/SpoT Homolog (RSH)-type proteins sense stress and control the cellular levels of the pleiotropically acting second messenger alarmone (p)ppGpp.

In Gram-positive bacteria, such as the model organism *Bacillus subtilis*, but also *Mycobacterium tuberculosis*, *Listeria monocytogenes*, and *Staphylococcus aureus*, nutrient limitation (i.e., amino acid starvation) is sensed by the RSH-type protein Rel, which recognizes uncharged tRNAs in the context of translationally stalled ribosome complexes (SRCs) to synthesize (p)ppGpp (Hauryliuk et al., 2015). Rel is a multi-domain protein that can be divided into an enzymatically active N-terminal domain (NTD) and a signal receptive and regulative C-terminal domain (CTD) (Figure 1A). The NTD consists of the $Mn^{2+}$-dependent hydrolase (Hyd) subdomain, which degrades (p)ppGpp to GTP/GDP and pyrophosphate ($PP_i$) in the absence of stress, and the $Mg^{2+}$-dependent synthetase (Syn) subdomain that catalyzes (p)ppGpp synthesis by transfer of $PP_i$ from ATP to the 3′-OH ribose of guanosine triphosphate (GTP)/guanosine diphosphate (GDP) when stalled ribosomes and uncharged tRNAs are sensed (Haseltine and Block, 1973; Haseltine et al., 1972; Sy and Lipmann, 1973). The CTD comprises four sub-domains, namely, the TGS (ThrRS, GTPase, and SpoT), AH (alpha helical), RIS (ribosome inter-subunit), and ACT (aspartate kinase, chorismate mutase, TyrA) (Figure 1A). The enzymatic activities of the NTD are regulated by the CTD such that, in the absence of the ribosome, the CTD inhibits synthesis and activates hydrolysis of (p)ppGpp by the NTD (Gropp et al., 2001; Jain et al., 2006; Mechold et al., 2002).

The molecular details of how the enzymatic activities within the NTD are regulated by the CTD remain enigmatic. Structural

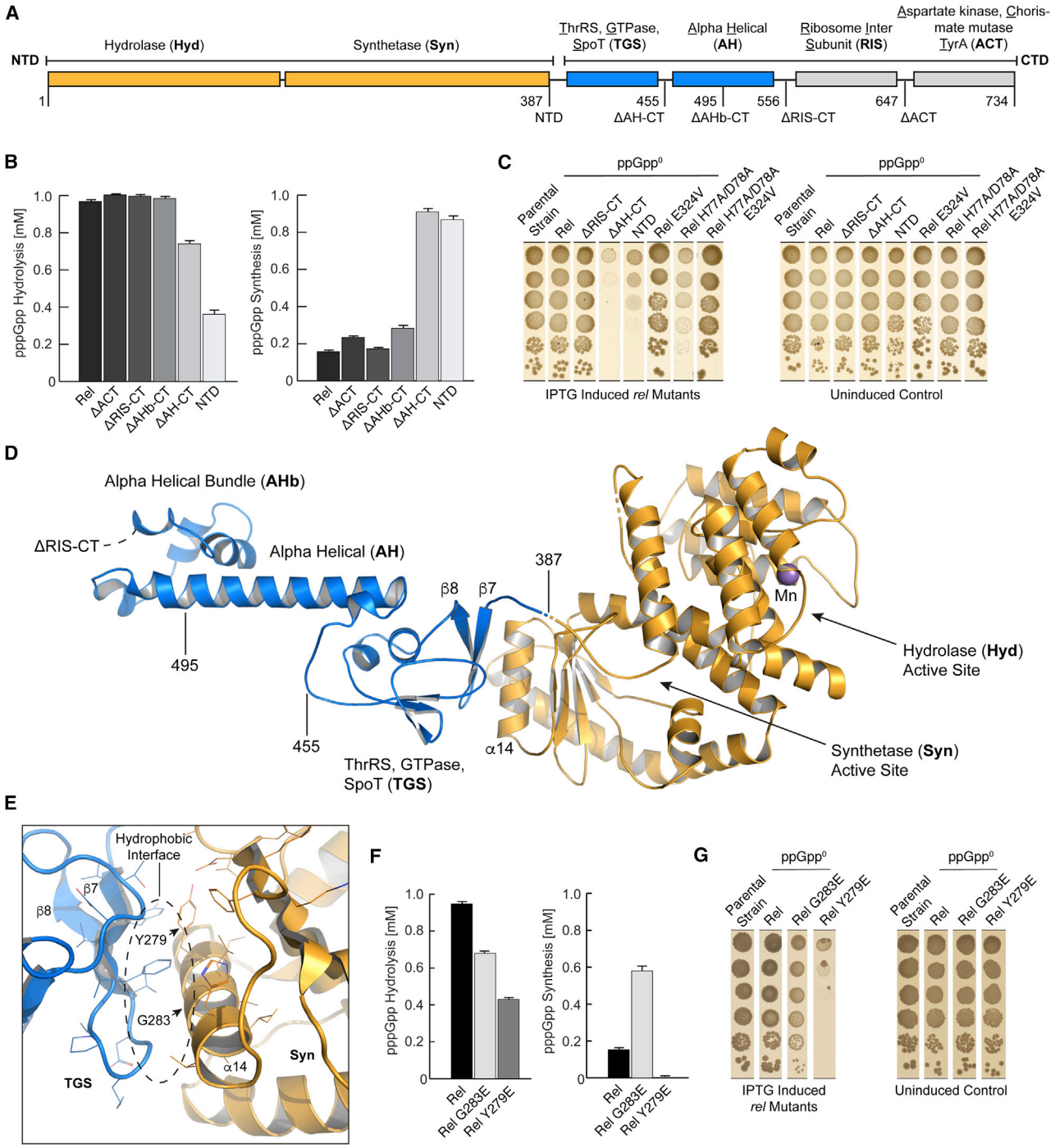


**Figure 1. The CTD of Rel Regulates Its Catalytic Activity**

(A) Domain architecture of Rel indicating its different subdomains. The N-terminal NTD, including the (p)ppGpp hydrolase and synthetase domains, is shown in orange. The CTD consists of the TGS and AH subdomains (both in blue) followed by the RIS and ACT domains (both in gray). The positions of the C-terminal deletions are indicated below.

(B) The *in vitro* pppGpp hydrolase and synthetase activities of different Rel variants are shown on the left and right sides, respectively (n = 2 technical replicates; means ± SD). Bars are color coded according to the respective truncation variant.

(C) *In vivo* growth assay of a *B. subtilis* ppGpp$^0$ strain expressing truncated variants of *rel* from an IPTG-inducible promoter. Reduced growth is induced by rising levels of (p)ppGpp (n = 2 biological replicates).

(D) Cartoon representation of the crystal structure of the RelΔRIS-CT. The NTD (hydrolase and synthetase domains) and the TGS/AH domains are shown in orange and blue, respectively.

*(legend continued on next page)*

data are available only for the homologous Gram-negative *Escherichia coli* RelA enzyme bound to the ribosome (Arenz et al., 2016; Brown et al., 2016; Loveland et al., 2016) and for the isolated NTDs of the Gram-positive *Streptococcus dysgalactiae* and *M. tuberculosis* Rel proteins in the absence of the regulative CTD (Hogg et al., 2004; Singal et al., 2017). Notably, the Gram-negative RelA protein contains an enzymatically inactive ''pseudo''-hydrolase subdomain instead of a functional hydrolase subdomain, as observed for Rel. Three cryoelectron microscopy (cryo-EM) studies of *E. coli* RelA bound to the ribosome in the presence of deacylated-tRNA revealed that RelA adopts an elongated ''open'' conformation to stimulate alarmone production by disrupting the proposed autoinhibitory interaction of the CTD with the NTD (Arenz et al., 2016; Brown et al., 2016; Loveland et al., 2016). In this extended conformation, RelA recognizes the deacylated CCA-3′ end of the A/R-tRNA (30S A-site/RelA bound) by the TGS domain and positions the NTD near the 30S spur for alarmone production. The TGS is C terminally followed by the AH domain, which wraps around the A/R-tRNA and connects to the RIS domain bridging the 50S and 30S subunits. The extreme C-terminal ACT domain folds back toward the A/R-tRNA and is buried in a cavity within the 50S subunit, formed by the A-site finger, helix 89, L16, and P-site tRNA. Exactly how RelA is capable of entering the ribosome to associate in this intricate conformation is unclear, but recent data suggest that RelA associates with the ribosome as a preformed RelA/deacylated-tRNA complex (Kushwaha et al., 2019a; Winther et al., 2018).

Upon dissociation from the ribosome and deacylated-tRNA, Rel was suggested to fall back in an inhibited NTD-CTD approximated ''closed'' conformation (Jain et al., 2006), which might also involve the oligomerization of Rel (Gropp et al., 2001; Yang and Ishiguro, 2001). The crystal structure of the NTD of *S. dysgalactiae* Rel revealed that it can adopt two conformations, namely, the Syn-ON/Hyd-OFF and Syn-OFF/Hyd-ON state for either alarmone synthesis or breakdown, respectively (Hogg et al., 2004). Based on these conformations, a reciprocal regulation of the antagonistic catalytic activities has been proposed that might involve a ligand-induced signal transmission between the Syn and Hyd active sites. However, an evaluation of this proposal is difficult because no structural data have visualized how the CTD could regulate the activity of the NTD in the absence of the ribosome.

Here, we set out to dissect the molecular mechanism of (p)ppGpp turnover control by the Rel protein from *B. subtilis*. We show by X-ray crystallography how the C-terminal TGS-AH subdomains associate to the Syn subdomain to repress (p)ppGpp synthesis in the absence of the ribosome. Our structural and functional analyses further reveal how (p)ppGpp hydrolysis is allosterically activated concomitant to association of the TGS. Moreover, we demonstrate that Rel forms homodimers, which appear to control the interaction with tRNA but not the enzymatic activity of Rel. Cryo-EM analysis of Rel bound to the stalled ribosome and deacylated tRNA reveals how alarmone synthesis is activated upon stress reception. Thus, our study provides a comprehensive molecular view on the Rel-dependent SR regulation in Gram-positive bacteria.

## RESULTS

### The TGS and AH Subdomains Are Critical for the Regulation of Rel

Rel from *B. subtilis* (*Bs*Rel) consists of the N-terminal hydrolase and synthetase domains, followed by its CTD consisting of the TGS, AH, RIS, and ACT domains (Figure 1A). To understand the regulatory impact of its CTD subdomain, we successively truncated *Bs*Rel domain-wise from the C terminus and assayed its (p)ppGpp synthetase and hydrolase activities *in vitro* by high-performance liquid chromatography (HPLC). Notably, all the *Bs*Rel variants contained a glutamate in place of histidine 420 (H420E) to avoid their co-purification with cellular tRNAs (see also Kushwaha et al., 2019; Winther et al., 2018). These experiments showed that the activity of *Bs*Rel (i.e., low (p)ppGpp synthetic and high (p)ppGpp hydrolytic activity) is maintained in the absence of the RIS and ACT subdomains, suggesting that both domains have no regulatory effect on the protein in the absence of the ribosome (Figure 1B). This interpretation agrees well with a previous study demonstrating that the RIS and ACT subdomains are dispensable for the regulation of *Bs*Rel in the absence of the ribosome (Jain et al., 2006). However, removal of the TGS and AH subdomains led to a pronounced increase in (p)ppGpp synthesis and a corresponding decrease in (p)ppGpp hydrolysis (Figure 1B). These results demonstrate that the critical regulative elements reside within the TGS and AH subdomains.

To consolidate these findings *in vivo*, we also evaluated the *Bs*Rel truncation variants in *B. subtilis* by using the cell-growth-reducing property of (p)ppGpp. To do so, we introduced the *rel* mutants in *trans* into the *amy* locus under the control of an (isopropyl-$\beta$-D-thiogalactopyranosid) IPTG-inducible promoter in a *B. subtilis* strain lacking (p)ppGpp synthetases and hydrolases (named (p)ppGpp$^0$ (BHS_214)). As controls for the enzymatic activity of *Bs*Rel, we included a (p)ppGpp synthetic inactive (E324V) and a (p)ppGpp hydrolytic inactive (H77A/D78A) variant, as well as a completely inactive (E324V and H77A/D78A) *Bs*Rel variant in our experimental setup. IPTG-induced production and growth analysis revealed that the *rel* knockout is functionally complemented by *rel* in *trans*, as well as by *Bs*Rel lacking the RIS and ACT subdomains (ΔRIS-CT) (Figure 1C). By contrast, we observed a prominent reduction in growth when we further truncated Rel by removing the AH and TGS subdomains (ΔAH and NTD) (Figure 1C). Western blotting revealed that all

(E) Detailed view on the interface between the Syn and TGS domains of Rel. Dashed lines indicate the position of the hydrophobic interface.
(F) The pppGpp hydrolase and synthetase activities of the Rel G283E and Y279E variants are shown on the left and right sides, respectively (n = 2 technical replicates; means ± SD).
(G) *In vivo* growth assay of a *B. subtilis* ppGpp$^0$ strain expressing *rel* variants G283E and Y279E from an IPTG-inducible promoter. Reduced growth is induced by rising levels of (p)ppGpp (n = 2 biological replicates).

**Table 1. Crystallographic Table for RelΔRIS-CT**

| Parameters | Data[a] |
|---|---|
| Space group | P $4_3$ $2_1$ 2 |
| Cell Dimensions | |
| *a*, *b*, *c* (Å) | 130.152 |
| | 130.152 |
| | 157.621 |
| α, β, γ (°) | 90.00 |
| | 90.00 |
| | 90.00 |
| Wavelength (Å) | 0.979 |
| Resolution (Å) | 46.82–3.95 |
| | (4.09–3.95) |
| No. of unique reflections | 12294 (1116) |
| Redundancy | 14.2 (13.1) |
| Completeness (%) | 99.06 (91.48) |
| $I/\sigma I$ | 10.04 (1.11) |
| $R_{merge}$ | 0.156 (1.908) |
| $R_{pim}$ | 0.043 (0.534) |
| CC(1/2) | 0.996 (0.497) |
| Refinement | |
| Reflections | 12,282 (1106) |
| Reflections ($R_{free}$) | 1,206 (93) |
| $R_{work}$ | 26.32 |
| $R_{free}$ | 28.22 |
| No. of atoms | 4,369 |
| Macromolecule | 4,368 |
| Ligand | 1 |
| Water | 0 |
| RMSDs | |
| Bond lengths (Å) | 0.003 |
| Bond angles (°) | 0.55 |
| Ramachandran (%) | |
| Preferred | 95.1 |
| Allowed | 4.9 |
| Outliers | 0.00 |
| Rotamer outliers (%) | 0.84 |

[a]Statistics for the highest-resolution shell are shown in parentheses.

complementing Rel variants were produced at levels comparable to the wild type (WT) (Figure S1A); hence, the growth defect should be attributed to elevated (p)ppGpp. As proxy for the intracellular (p)ppGpp concentration, we determined the levels of the ribosome hibernation promoting factor HPF (YvyD), the synthesis of which correlates with the cellular (p)ppGpp (Beckert et al., 2017; Schäfer et al., 2020; Tagami et al., 2012). The occurrence of HPF in strains expressing different variants of *rel* strongly correlated with the (p)ppGpp synthesis by those variants determined *in vitro* (Figures S1B and S1C). Taken together, our results show that TGS and AH provide the major elements regulating the reciprocal (p)ppGpp synthetase and hydrolase activities of Rel.

## Crystal Structure of *B. subtilis* Rel

Next, we wanted to obtain structural insights into the TGS- and AH-dependent regulation of Rel. Because the ACT and RIS domains are dispensable for the regulation of Rel activity (see previous section), we used a Rel variant lacking these domains (RelΔRIS-CT). The crystal structure of RelΔRIS-CT was determined by molecular replacement (MR) using the structure of *S. dysgalactiae* Rel-NTD (*Sd*Rel-NTD) (PDB: 1VJ7; Hogg et al., 2004) and refined to a resolution of 3.95 Å (Table 1). The resolution was sufficient to place the secondary structure elements of the Syn, Hyd, TGS, and AH domains of Rel into the electron density map (Figures S2A and S2B). The structure revealed nucleotide-free *Bs*Rel in an elongated conformation in which the TGS domain contacts the Syn domain by an interface involving α-helix 14 and β strands 7/8 of the Syn and TGS domains, respectively (Figure 1D). Analysis of the interface by the program PISA (Krissinel and Henrick, 2007) revealed that the TGS-Syn interaction interface involves an area of 505.5 $Å^2$ and is characterized by a calculated $\Delta^iG$ of −10.5 kcal/mol (p = 0.046), arguing for a largely hydrophobic and specific interaction interface (Figure 1E).

To validate our structural findings, we introduced single-amino acid substitutions in the Syn/TGS interface to interfere with the association of the TGS to the Syn domain. We varied glycine 283 or tyrosine 279, which are located central to the interface in helix α14 of the Syn subdomain, to glutamate for disruption of the hydrophobic core of this interface (Figure 1E). We then used our *in vitro* and *in vivo* assays to analyze the effect of these substitutions on the activity of Rel. Both assays revealed that the G283E Rel variant protein is indeed deregulated, as evidenced by its high (p)ppGpp synthetic and reduced (p)ppGpp hydrolytic activity (Figures 1F and 1G). Interestingly, Y279E was inactive in (p)ppGpp synthesis *in vitro*, but not *in vivo*, suggesting that this mutation destabilizes the Syn domain *in vitro* (Figures 1F and 1G). However, the Y279E variant also resulted in a pronounced reduction in hydrolase activity, arguing for deregulated enzymatic activities. Both variants eluted as a single peak during size exclusion at a similar retention time, demonstrating that the overall folding was not affected by the amino acid variations (Figure S3). Taken together, our mutational analysis supports the hypothesis that the association of the TGS and Syn subdomains in *cis* are critical for the regulation of the (p)ppGpp synthetase and hydrolase activities of Rel.

## The TGS Domain Regulates the Reciprocal Activities of Rel

Next, we compared the NTD conformation of our *Bs*RelΔRIS-CT structure to the available NTD structures of *Sd*Rel-NTD (60% amino acid identity) in the proposed Hyd-ON/Syn-OFF and Hyd-OFF/Syn-ON conformations (Figures 2A and 2B). The structural comparison revealed that the NTD conformation of *Bs*RelΔRIS-CT best matches the proposed Hyd-ON/Syn-OFF conformation of *Sd*Rel-NTD (root-mean-square deviation [RMSD], 0.649), when compared to the *Sd*Rel-NTD Hyd-OFF/Syn-ON conformation (RMSD, 1.107). Thus, our structural comparison supports the interpretation of the NTD conformations observed by Hogg et al. (2004) for the isolated NTD structures of *Sd*Rel and suggests, likewise, that the NTD of *Bs*RelΔRIS-CT exists

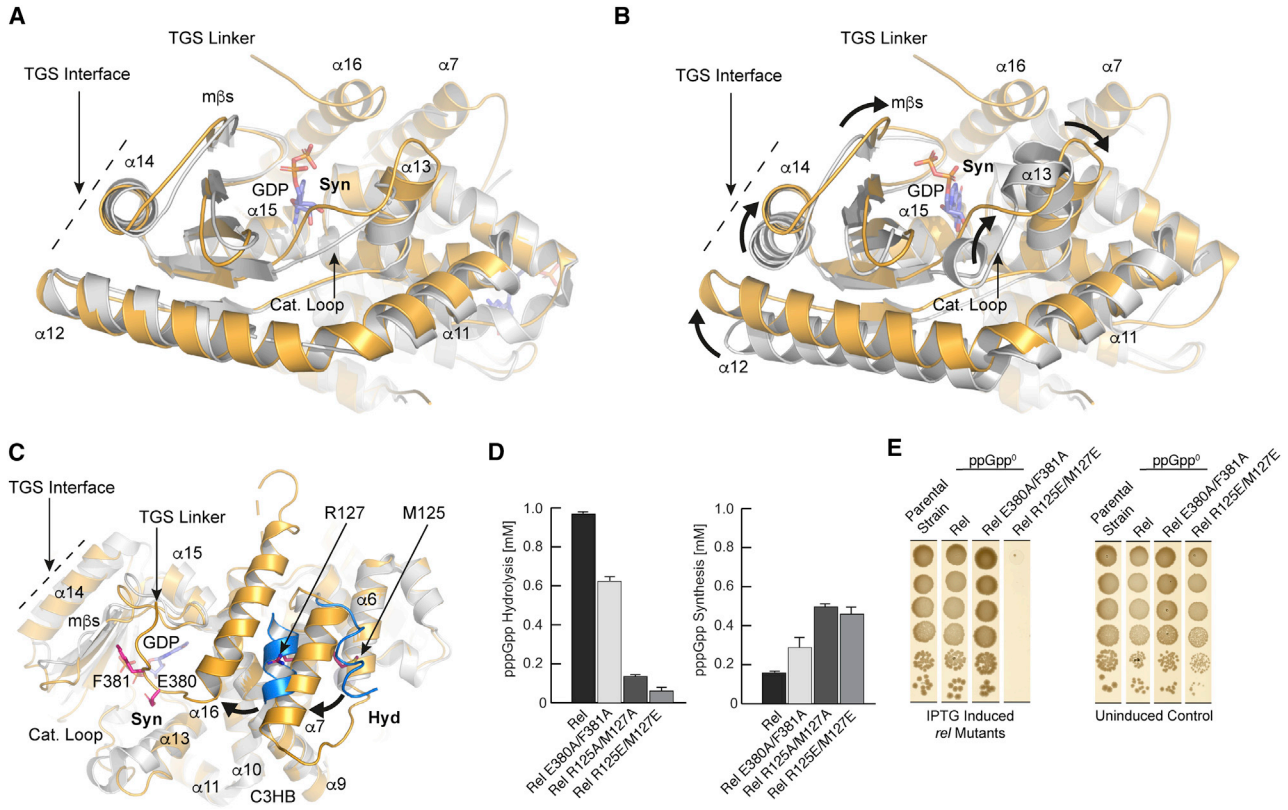


**Figure 2. The Enzymatic Activity of Rel Is Switched by Structural Rearrangements Transmitted within the NTD**

(A and B) Syn-domain-centered view of the superimposition of the *Bs*Rel crystal structure NTD domain (orange) with the *Sd*Rel crystal structures (gray) in the proposed Hyd-ON/Syn-OFF (shown in A; PDB: 1VJ7; chain B) and Hyd-OFF/Syn-ON (shown in Bb; PDB: 1VJ7; chain A), aligned by α helices 8–10. Arrows indicate structural rearrangements that are observed between the Syn-ON and Syn-OFF state.

(C) Top view of the *Bs*Rel (orange) and *Sd*Rel (gray; Hyd-OFF/Syn-ON conformation) superimposition. *Sd*Rel α helices 7 and 16 are shown in blue, and arrows illustrate replacements of the helices. Residues selected for variation are shown in pink.

(D) *In vitro* pppGpp hydrolysis and synthesis activity of WT-Rel and Rel variants containing amino acid substitutions in the TGS linker and α helices 7 and 16 (n = 2 technical replicates; means ± SD).

(E) *In vivo* growth assay of a *B. subtilis* ppGpp$^0$ strain expressing *rel* variants from an IPTG-inducible promoter. Reduced growth is induced by rising levels of (p)ppGpp (n = 2 biological replicates).

in the Hyd-ON/Syn-OFF state in our crystal structure. The structural comparison further revealed how the active sites are remodeled upon association of the TGS subdomain. Association of the TGS to helix α14 and the central mixed β sheet of the Syn domain leads to an orchestrated movement of helices α14 and α15 and the mixed β sheet along helix α12, resulting in displacement of the catalytic loop and helix α13 (Figure 2B), which are essential for $Mg^{2+}$ binding and association of ATP for $PP_i$ transfer to GTP/GDP (Hogg et al., 2004). Thus, the synthetase becomes remodeled and repressed upon association of the TGS.

Unexpectedly, our structural comparison further revealed that two α helices (α7 and α16) become stabilized in between the Hyd and Syn subdomains on top of the central three-helical bundle (C3HB; α8-α10), which connects both subdomains (Figure 2C). The stabilization of helices α7 and α16 seems to be facilitated by helix α16 that is directly connected by a short linker region to the TGS domain. Hence, helix α16 and the adjacent helix α7 might rearrange upon association of the TGS to the Syn (Figure 2C). Because helices α7 and α16 directly connect the Syn and Hyd subdomains, those elements represent good candidates to mediate the allosteric regulation of the Hyd. Furthermore, the rearrangement of helix α16 leads to association of the TGS-connecting linker close to the Syn active site, which might assist in repression of the synthetase activity. To test the involvement of helices α7 and α16 in the regulation of Rel, we introduced amino acid variations in the linker region (E380A/F381A) and in helix α7 (R125A/M127A; R125E/M127E) to interfere with the association of those elements (Figure 2C). We again used our *in vitro* and *in vivo* assays to analyze the effect of those variations on the activity of Rel. Both assays revealed that the E380A/F381A variant Rel protein was only slightly deregulated in its activity, whereas the Rel R125A/M127A and R125E/M127E variant enzyme activity was strongly affected by the amino acid substitution in helix α7, as suggested by a pronounced repression of the hydrolase and activation of the synthetase activities (Figures 2D and 2E). Thus, the rearrangement of helices α7 and α16 appears to facilitate the allosteric

regulation of the hydrolase upon association of the TGS to the synthetase. Taken together, our data show that the TGS domain regulates the enzymatic activities in the NTD by association to and remodeling of the Syn subdomain. Furthermore, helices α7 and α16 seem to control the reciprocal activities within the NTD by allosterically communicating the TGS association to the Hyd subdomain.

### Ability of Rel to Homodimerize

Inspection of the crystal packing revealed a Rel homodimer, which forms across the crystallographic two-fold axis (Figure 3A; Figures S2A and S2B). Within the symmetric Rel homodimer, each monomer contacts the other through interactions between the TGS-AH subdomains and the NTD. The loop connecting helices α17 and α18 of the TGS domain of one monomer interacts with the loop connecting helix α12 and strand β3 of the Syn domain of the other and vice versa (Figure 3A). Helices α19 and α20 of the AH domain of one monomer binds into an extended surface cavity formed by helices α1/α3 of the Hyd and helix α15 and the sheet β3/4 of the Syn of the other (hereafter referred to as NTD-cleft) and vice versa. The interaction interface seems to be primarily established by polar interactions of the positively charged TGS-AH subdomains and the negatively charged NTD-cleft (Figure 3B). Interface analysis with the program PISA (Krissinel and Henrick, 2007) revealed that the interaction interface comprises a total area of 1,757.4 $Å^2$ and is characterized by a calculated $\Delta^iG$ of 0.6 kcal/mol (p = 0.802), demonstrating that the interface is mainly established by polar interactions (hydrogen bonds: 20; salt bridges: 4). It is important to note that p values of >0.5 imply that the interface is less hydrophobic than it could be in respect to the total area and may thus be an artifact of crystal packing.

Nevertheless, we introduced charge-reversing amino acid substitutions in the NTD-cleft (E65R, F330R, E334R, and E65R/F330R/E334R) and analyzed the activity of Rel in our *in vivo* and *in vitro* assays (Figures 3C and 3D). The analysis revealed that neither of the amino acid substitutions affected the activity of Rel (Figures 3C and 3D). To analyze if the variant Rel proteins were indeed impaired in the interaction of the NTD-cleft with the TGS-AH subdomain, we individually purified glutathione S-transferase (GST)-tagged and CTD-truncated NTD variant proteins to reconstitute the NTD/TGS-AH interaction *in vitro* in a GST pull-down experiment by using purified TGS-$AH^{H420E}$ fragments as prey (Figure 3E). Interestingly, we observed that the interaction of GST-$NTD^{WT}$ with the TGS-AH was highly dependent on the salt concentration of the buffer used during the pull-down experiment (Figure S4A). Buffers containing >100 mM NaCl resulted in a robust decrease in pull-down efficiency, which again argues for an interface that is largely established by polar interactions. The pull-down experiments revealed that although the GST-$NTD^{WT}$ was capable of interacting with the TGS-$AH^{H420E}$ fragment, the E65R, F330R, E334R, and E65R/F330R/E334R variant GST-NTD proteins were impaired in their interaction, showing that the NTD/TGS-AH interaction is prohibited in these variants (Figure 3E). This observation in combination with the activity assays suggests that the observed homodimer interaction does not contribute to the regulation of the enzymatic activities of Rel.

### The ACT Subdomain Contributes to the Stability of the Rel Homodimer

Next, we aimed to understand the dimer interaction of Rel in greater detail. We therefore set up an *in vivo* bacterial two-hybrid (B2H) assay. The B2H assay revealed that full-length Rel was capable of interacting with full-length Rel (Figure 4A). Deletion of the RIS and ACT domains (RelΔRIS-CT) resulted in decreased interaction strength in our B2H setup, suggesting that these domains might contribute to dimer formation (Figure 4A). Furthermore, the individual TGS-AH fragments did not interact with themselves, demonstrating that these subdomains are not capable of mediating dimer contacts in the absence of the NTD.

To cross-validate our *in vivo* interaction study *in vitro*, we performed a bio-layer interferometry (BLI) analysis of purified $Rel^{H420E}$ truncation variants to determine the dissociation constants ($K_D$) and the contributing $k_{on}$ and $k_{off}$ values (Figure 4B; Figure S4B; Table S1). Full-length Rel and RelΔRIS-CT interacted with $K_D$s of ≈10.6 ± 0.2 μM and ≈4.9 ± 0.01 μM (Figure 4B). No relevant self-interaction of TGS-AH domain was observed (i.e., $K_D$ of ≈129 ± 7 μM), showing that that TGS-AH does not interact in solution (Figure 4B). Although our analysis suggested a self-interaction of the NTD with a $K_D$ of ≈43.1 ± 3.3 μM, a comparison of the $k_{on}$ (≈7.5 ± 0.5 $M^{-1}s^{-1}$) and $k_{off}$ (3.2 × $10^{-4}$ ± 7.5 × $10^{-6}$ $s^{-1}$) showed that any NTD homodimer formed is extremely short lived (Figure 4B). The structure of the Rel homodimer also suggested that the NTD should be capable of interacting with the TGS-AH, first, by the TGS in *cis*, and, second, by the TGS-AH in *trans*. Indeed, analysis of the interaction between the NTD and TGS-AH revealed two distinct $K_D$ values in the low micromolar range ($K_{D1}$ ≈4.8 ± 0.1 μM and $K_{D2}$ ≈10.7 ± 0.2 μM) and a stoichiometry of one NTD with two TGS-AHs (Figure 4B).

Next, we performed analytical size-exclusion chromatography coupled with multi-angle light scattering (SEC-MALS) as an absolute method to determine the molecular weight and thereby the oligomerization state of the analyzed protein. SEC-MALS of full-length WT Rel revealed a molecular weight of approximately 200 kDa, which is close to the expected molecular weight of a Rel homodimer (171.3 kDa) (Figure 4C). When we subsequently analyzed the molecular weights of the CTD subdomain truncations, we found that already upon truncation of the ACT domain, the homodimeric state is lost (Figure 4C). Hence, the ACT domain seems to contribute to dimer formation, which is in line with our *in vivo* B2H assay that revealed reduced interaction strength in the absence of the ACT (Figure 4A). It is important to note that most Rel variants (full length, ΔACT, ΔRIS-CT, and ΔAH-CT) require high concentrations of NaCl during SEC (>500 mM, optimally 1 M NaCl) to prevent aggregate formation. As we have shown in the GST pull-down experiments, the NTD-cleft/TGS-AH dimer interaction is facilitated mainly by polar contacts and highly susceptible to high concentrations of NaCl. Hence, formation of the dimer, exclusively by this interface, might not be observed under the conditions required to retain Rel in solution for SEC-MALS. In summary, Rel homodimer formation seems to be mediated, first, by the polar NTD-cleft/TGS-AH interface and, second, by dimer stabilization through the ACT subdomain.

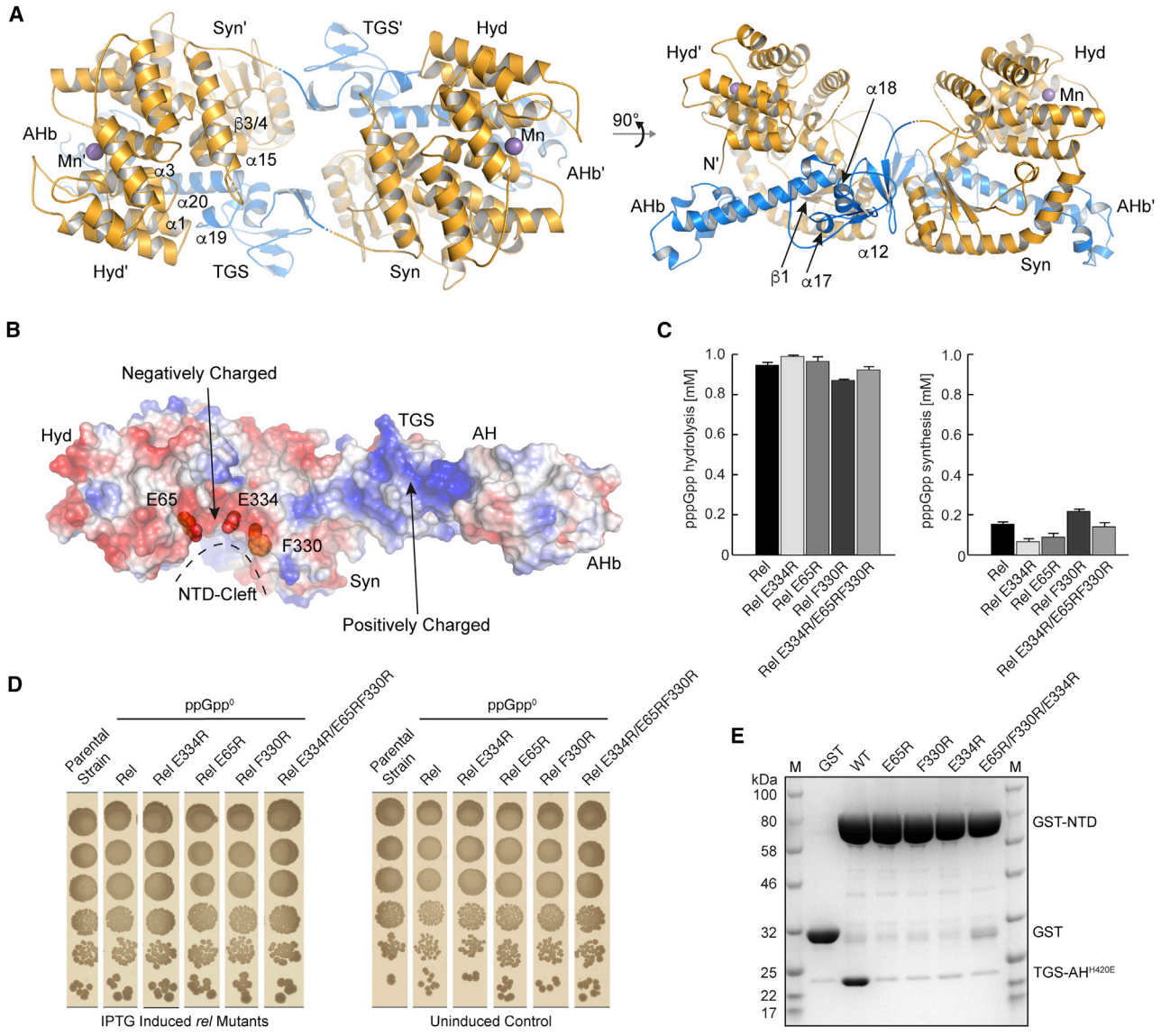


**Figure 3. Rel Forms a Crystallographic Homodimer**

(A) Rel forms a homodimer across the crystallographic 2-fold axis. One monomer is shown in blue and the other in orange.

(B) The positively charged TGS-AH domain of one monomer interacts with a negatively charged surface groove present in the NTD domain of the other monomer and vice versa.

(C) *In vitro* pppGpp hydrolysis and synthesis activities of WT-Rel and Rel variants containing amino acid substitutions within the negatively charged cleft at the NTD (n = 2 technical replicates; means ± SD).

(D) *In vivo* growth assay of a *B. subtilis* ppGpp$^0$ strain expressing *rel* variants from an IPTG-inducible promoter. Reduced growth is induced by rising levels of (p)ppGpp (n = 2 biological replicates).

(E) Coomassie-stained SDS-PAGE of an *in vitro* pull-down assay using the GST-tagged NTD as bait and wild-type TGS-AH and its variants as prey (this experiment was performed once).

## Homodimer Formation of Rel Antagonizes the Rel tRNA-Binding Ability

When we compared the homodimeric structure of Rel to the published cryo-EM structures of *E. coli* RelA (*Ec*RelA) (Arenz et al., 2016; Brown et al., 2016; Loveland et al., 2016), we were intrigued by the apparent masking of the deacylated tRNA-binding site at the TGS-AH subdomains in the context of the homodimer (Figure 4D). Hence, we speculate that, although the dimer formation might not control the activities in the NTD, the dimer might impact the interaction with tRNA. To test this idea, we set up a pull-down experiment to analyze the interaction in dependence of the presence of the tRNA species interacting with Rel ($tRNA^{Rel}$). The $tRNA^{Rel}$ was prepared from a TGS-$AH^{WT}$ fragment by extraction with TRIzol. RNA-free TGS-$AH^{WT}$ was prepared by treatment with RNase A and high-salt washing (i.e., 2 M NaCl). The pull-down experiment revealed that

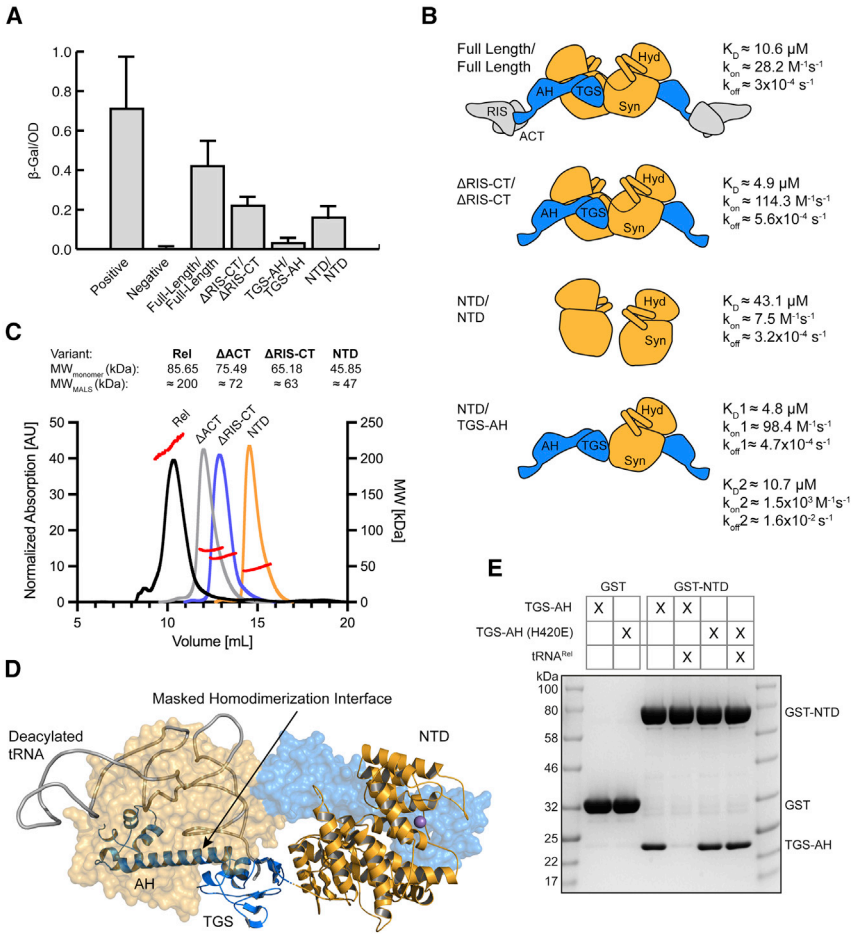


**Figure 4. Homodimerization of Rel Overlaps with Its Ability to Bind tRNA**

(A) Bacterial two-hybrid assay of WT-Rel and its variants (n = 6 biological replicates; means ± SD).

(B) Interaction parameters of purified Rel variants as derived from bio-layer interferometry. Only interactions with a $K_D$ < 50 μM are shown (n = 2 technical replicates).

(C) Size-exclusion chromatography (as measured at 280 nm) and MALS-RI analysis (calculated molecular weights [MWs] are shown as red lines) of WT-Rel and its truncation variants (this experiment was performed once). The theoretical MW of a monomer ($MW_{monomer}$) and the MW determined by MALS-RI ($MW_{Mals}$) are given in kDa.

(D) The tRNA (gray) binding site of Rel is hidden within the interface of the Rel homodimer.

(E) Coomassie-stained SDS-PAGE of an *in vitro* pull-down assay using the GST-tagged NTD as bait and wild-type TGS-AH and its H420E variant prey in the presence and absence of tRNA (this experiment was performed once).

TGS-AH$^{WT}$ and TGS-AH$^{H420E}$ were both capable of interacting with the GST-NTD protein in the absence of tRNA$^{Rel}$ (Figure 4E). Upon addition of a 1.5-fold excess of tRNA$^{Rel}$, we observed a pronounced loss of interaction for the TGS-AH$^{WT}$ fragment but not for the TGS-AH$^{H420E}$ fragment (Figure 4E). This finding shows that the interaction is impaired in the presence of tRNA$^{Rel}$ for the WT subdomains. Furthermore, this demonstrates that histidine residue 420 is critical for the interaction of the TGS-AH subdomains with the recognized tRNA$^{Rel}$, as the H420E variant does not allow interaction with tRNA$^{Rel}$ (Kushwaha et al., 2019; Winther et al., 2018). Hence, formation of the Rel dimer by the NTD-cleft/TGS-AH interface is incompatible with the interaction of the TGS-AH subdomain with tRNA$^{Rel}$.

## Mono- and Bifunctional RSH Enzymes Share Their Activation Mechanism on the Ribosome

To analyze how the bifunctional *B. subtilis* Rel senses the stress signal, we assembled and analyzed a *B. subtilis* Rel·stalled ribosomal complex (Rel·SRC) using single-particle cryo-EM, similarly to that described previously for the *E. coli* RelA·SRC. The *B. subtilis* SRC was obtained using a disome purification protocol based on a dicistronic mRNA encoding an R8K variant of the ErmDL stalling leader peptide (Figure S5). The *B. subtilis* Rel·SRCs were formed by incubating the *B. subtilis* ErmDL R8K·SRC with deacylated tRNA$^{Lys}$ and purified recombinant *B. subtilis* Rel protein in the presence of GDP and the non-hydrolyzable ATP analog α, β-methylene-ATP. The cryo-EM data for the *B. subtilis* Rel·SRC were collected on a Titan Krios microscope with a Falcon II direct electron detector. From a total of 650,054 ribosomal particles, 3D classification revealed a diverse array of ribosome subpopulations containing only P-sitetRNA (8.9%), E-sitetRNA (12.5%), and both P- and E-site tRNAs (25.3%), as well as A- and P-site tRNAs with (33.4%) and without (9.1%) E-tRNA (Figure S5F). Despite this vast heterogeneity, it was also possible to obtain a small subpopulation (10.3%) that contained P- and E-tRNAs, as well as A/R-tRNA and Rel bound within the ribosomal A-site (Figure S5F). This subpopulation could be further refined to yield a final cryo-EM map of the *B. subtilis* RelA·SRC (Figure 5A; Table S2) with an average resolution of 4.5 Å (Figure S6A) and local resolution reaching to 3.8 Å within the core of the ribosome (Figures S6B and S6C). Local resolution calculations for the A/R-tRNA and Rel ranged from 5–7 Å (Figures S6D and S6E), consistent with the high flexibility of the A/R-tRNA and Rel within the ribosomal binding site, as observed previously for the *E. coli* RelA·ribosome complexes (Arenz et al., 2016; Brown et al., 2016; Loveland et al., 2016). The resolution allowed an unambiguous rigid body fit of homology models for the *B. subtilis* Rel TGS, RIS, and ACT domains to the cryo-EM density, together with the A/R-tRNA (Figure S6). The density for the AH linker connecting the TGS and RIS of *B. subtilis* Rel was relatively well resolved and most consistent with the conformation observed in the *E. coli* RelA model from Loveland et al. (2016) (Figure S6). The overall conformation of *B. subtilis* Rel and the A/R-tRNA on the *B. subtilis* 70S ribosome is analogous to that observed previously for the *E. coli* RelA·ribosome complexes (Arenz et al., 2016; Brown et al., 2016; Loveland et al., 2016;

Figures 5B and 5C). Also, the individual domains of *B. subtilis* Rel appear to establish a similar set of contacts with the ribosome, such that the TGS domain interacts with the CCA end of the deacylated A/R-tRNA and with h5/h15 of the small subunit; the ACT domain interacts with H38, L16, and H43 of the large subunit; and the RIS bridges both subunits by interaction with H38 and S19 (Figure S7). The NTD was poorly ordered in the *B. subtilis* Rel·SRC, but additional density could be seen when the map was filtered to 12 Å in a similar but distinct position to that observed previously for the *E. coli* RelA·ribosome complexes (Figure S7). Hence, (p)ppGpp synthesis might be triggered by detraction of the inhibitory CTD from the NTD upon ribosome contact, which was also suggested for the *Ec*RelA protein (Arenz et al., 2016; Brown et al., 2016). A comparison of the SRC-associated state and the ribosome and deacylated tRNA-free state further revealed that the CTD undergoes a large rearrangement relative to the NTD (TGS: 50 Å; AH: 125 Å) upon association with the SRC (Figure 5D). Furthermore, an association of the SRC and deacylated A/R tRNA results in bending of α-helix 20 of the AH subdomain, which would be incompatible with Rel homodimer formation (Figure 5D). Strikingly, α helices 7 and 16, which relay the Syn and Hyd active sites, become rearranged upon SRC contact, likely to activate (p)ppGpp synthesis and to repress (p)ppGpp hydrolysis.

Taken together, our structural analysis revealed that the regulation of the RSH-type enzymes RelA and Rel by the SRC seems very similar in that detraction of the CTD allows for stimulation of (p)ppGpp synthesis. Moreover, the comparison to our structure of Rel in the SRC-free state suggests that this activity switch is due to the removal of the TGS subdomain from the Syn domain and the concomitant rearrangement of α helices 7 and 16 to activate the synthetase and repress the hydrolase.

## DISCUSSION

### Regulation of the Enzymatic Activities of Rel by Its CTD

In the absence of stress signals, i.e., deacylated tRNA, the (p)ppGpp synthetic activity of Rel needs to be repressed and the (p)ppGpp hydrolytic activity must be stimulated to clear the cell of the growth-inhibiting (p)ppGpp nucleotides. Our structure of *B. subtilis* Rel revealed that to facilitate this regulation, the C-terminal TGS subdomain associates to the N-terminal Syn subdomain to remodel the active site for repression of (p)ppGpp synthesis. Furthermore, we could show that the Syn subdomain and its activity are relayed by an allosteric signal transmission route formed by helices α7 and α16 to the Hyd subdomain for reciprocal regulation of both activities. Due to the low resolution of our crystal structure, which is likely owed to the intrinsic flexibility of Rel, we were not able to unambiguously delineate side-chain rearrangements that might contribute to the activity switch in Rel. A previous study revealed two conformations in the high-resolution crystal structure of the *Sd*Rel-NTD in absence of the CTD, which might correspond to the Syn-ON/Hyd-OFF and Syn-OFF/Hyd-ON state (Hogg et al., 2004). Our study confirmed that the Syn-OFF/Hyd-ON conformation observed by Hogg et al. (2004) approximates the Syn-OFF/Hyd-ON conformation the in presence of the regulative CTD TGS-AH subdomains. Notably, Hogg et al. (2004) did not observe the rearrangements of helices α7 and α16 in the absence of the regulative CTD. This implies that correct association of helices α7 and α16 for the formation of the Syn-OFF/Hyd-ON conformation requires the interaction of the TGS with the Syn domain. Furthermore, the Syn-OFF/Hyd-ON conformation observed by Hogg et al. (2004) seems to be fostered by crystal packing, as the individual NTD fragment adopts the Syn-ON/Hyd-OFF state in the absence of the CTD in solution. While our manuscript was under review, a study on the N-terminal Rel fragment from *Thermus thermophilus* revealed the importance of helices α7 and α6 in the allosteric switch and formation of the hydrolase active site (Tamman et al. 2020). This observation supports the idea that helices α7 and α16 constitute the allosteric regulation route in Rel that signals for TGS association to the Syn subdomain. In summary, we revealed that TGS-AH directly interacts with the NTD in the absence of stress to switch Rel's (p)ppGpp synthetic and hydrolytic activities by remodeling of the active sites.

### The Rel Homodimer Controls tRNA Reception but Not the Enzymatic Activity

We could show that Rel homodimerization is mediated by two elements: first, by the NTD-cleft/TGS-AH interface, and second, by stabilization of the dimer by the ACT subdomain. We further demonstrated that dimer formation is incompatible with the association of $tRNA^{Rel}$. Hence, the homodimeric state of Rel might control the interaction with tRNA or vice versa. Notably, we could demonstrate that the homodimer does not affect the enzymatic activity of Rel. Amino acid substitutions in the NTD-cleft/TGS-AH interface that abrogate the interaction did not alter the activity of Rel. Furthermore, truncation of the ACT, as well as the truncation of the RIS and ACT, did result in the loss of homodimerization but did not affect the enzymatic regulation of Rel *in vitro* and *in vivo*. Homodimerization of the Rel homologous RelA protein from *E. coli* has been reported previously and was shown to involve two regions, namely, the TGS-AH (amino acids 455–538) and the AH-ACT subdomains (amino acids 550–682) (Gropp et al., 2001; Yang and Ishiguro, 2001). Although these two regions correspond to the regions that we also identified to be crucial for homodimer formation, the homodimerization mechanism of *E. coli* RelA might be distinct from the homodimerization observed for *B. subtilis* Rel. Homodimerization of *Ec*RelA has been suggested to occur exclusively by direct CTD/CTD interactions and may not involve an interaction of the CTD with the NTD (Gropp et al., 2001; Yang and Ishiguro, 2001). Future studies will need to clarify the biological significance of the two distinct dimerization modes of Rel and RelA.

Interestingly, and in contrast to the regulation of *Bs*Rel, the CTD-mediated oligomerization of *Ec*RelA has been proposed to regulate the activity of *Ec*RelA, as overexpression of the individual CTD fragment results in an attenuated SR (Yang and Ishiguro, 2001). However, overexpression of the individual CTD directly competes with the association of full-length *Ec*RelA with the ribosome, prohibiting SRC interaction and thereby preventing (p)ppGpp synthesis (Takada et al., 2020; Turnbull et al., 2019). This idea is also supported by the property of the CTD

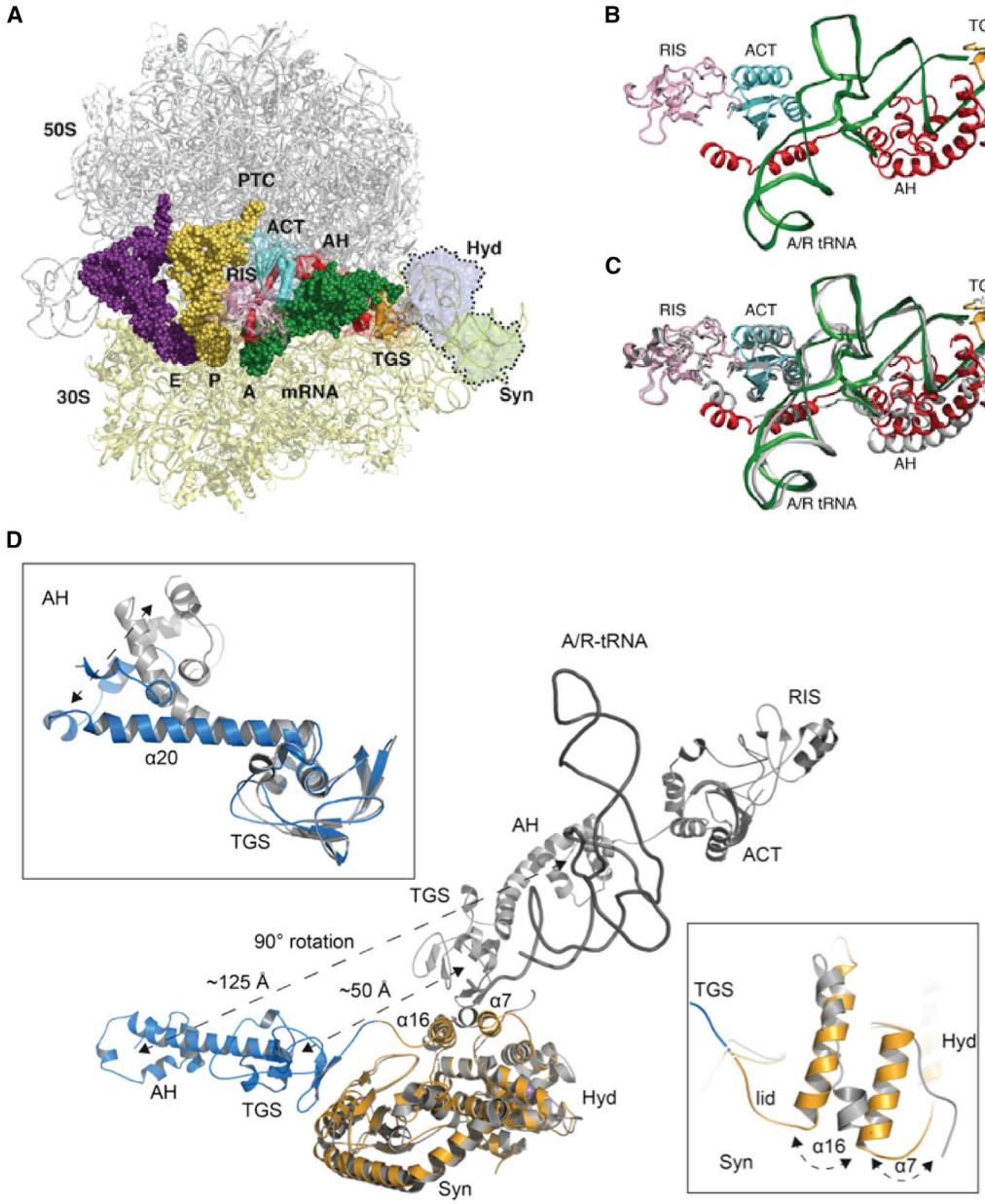


**Figure 5. Cryo-EM Structure of the *B. subtilis* Rel-SRC**

(A) Cryo-EM structure of the *Bs*Rel-SRC. The 50S (gray), 30S (beige), and *Bs*Rel are shown in cartoon representation. The dot-framed transparent region indicates the estimated configuration of the NTD. The A/R-site tRNA (green), P-site tRNA (yellow), and E-site tRNA (purple) are shown in sphere representation.

(B and C) Isolated view on the *Bs*Rel-tRNA conformation on the ribosome and comparison of the conformation (C) shown in (B) to the conformation observed for *Ec*Rel-A/R-tRNA on the ribosome (gray).

(D) Comparison of the structure of ribosome-dissociated *Bs*Rel (this study, blue and orange) to the ribosome-bound structure of *Ec*RelA (PDB: 5KPV). Arrows indicate large structural rearrangements of the CTD between the two states. The insets highlight structural rearrangements in the AH domain (top left) and α helices 7 and 16 (bottom right).

to interact with ribosomes, as evident from the *Ec*RelA·SRC cryo-EM structures (this study; Arenz et al., 2016; Brown et al., 2016; Loveland et al., 2016) and by the observation that the CTD co-sediments with ribosome fractions (Yang and Ishiguro, 2001). Hence, the activity of the *Bs*Rel-homologous *Ec*RelA protein might not necessarily be influenced by homodimerization. In summary, although the homodimeric state of Rel does not seem to contribute to the enzymatic activity regulation, it may control tRNA interaction. Future studies will be needed to address the biological significance underlying this observation in respect to the exact order of events that lead to homodimer dissociation and its influence on SR signaling.

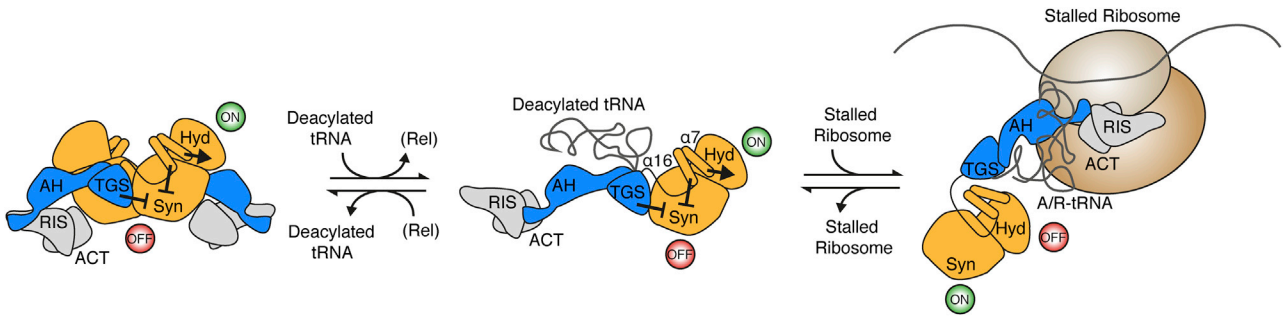


**Figure 6. Mechanism of Rel Regulation**

During relaxed conditions, i.e., high availability of amino acids and low abundance of deacylated tRNAs, Rel might reside in a homodimeric Hyd-ON/Syn-OFF state (left). Upon reception of deacylated tRNAs, Rel might monomerize. The Rel●deacylated-tRNA complex is formed, which is competent to recognize the SRC but remains in the Hyd-ON/Syn-OFF state (middle). Stringent conditions (amino acid starvation) result in an increase of deacylated tRNAs, priming Rel for interaction with translationally stalled ribosomes that present a matching A-site codon. Accommodation of the CTD in the SRC leads to the activity switch in the NTD for alarmone production and SR signaling (right).

### (p)ppGpp Synthesis Is Triggered on the Ribosome by Disrupting the CTD-NTD Interaction

Upon nutrient limitation, Rel needs to interact with the SRC to switch its activities for (p)ppGpp synthesis and SR signaling. Our crystal structure of ribosome-free Rel and our cryo-EM structure of the Rel·SRC revealed that upon Rel recruitment by the SRC, the inhibitory CTD is detached from the NTD to allow for alarmone synthesis (Figure 5D). Dissociation of the TGS subdomain from the Syn subdomain allows the NTD to adopt the Syn-ON/Hyd-OFF for (p)ppGpp production. This rearrangement seems to be facilitated by the removal of the structural constraints that the TGS imposes on the Syn, when associated with helix α14 of the Syn subdomain. Furthermore, rearrangement of helices α7 and α16 become displaced from the C3HB, and subsequently, the Hyd might become destabilized to silence its (p)ppGpp hydrolytic activity in the presence of the SRC. Furthermore, our cryo-EM structure of the Rel·SRC revealed that the established interactions of Rel with the SRC are highly similar to the SRC interaction observed for the homologous RelA protein from *E. coli* (Figures 5B and 5C). Therefore, our findings suggest that the ribosome-dependent activation of the Syn activity of *E. coli* RelA uses an analogous mechanism to that observed here. Due to the extent of structural similarity, we further envisage that the inhibition of *E. coli* RelA occurs analogously to *B. subtilis* Rel in the absence of the SRC by association of the TGS with the Syn domain. One major difference between Rel and RelA is that Rel contains a functional Hyd domain, while RelA carries an inactive pseudo-hydrolase domain. Therefore, ribosome binding in the case of Rel leads not only to stimulation of the Syn activity but also inactivation of the Hyd domain. In the structure of the *B. subtilis* Rel·SRC determined here, the NTD exhibited a high degree of flexibility, suggesting no obvious stabilizing interactions existing with the ribosome (Figure S7). Therefore, we favor a model whereby activation of Syn allosterically inactivates the Hyd (Hogg et al., 2004), rather than inactivation of the Hyd by additional interactions with components of the ribosome. In this regard, we note that the sarcin-ricin loop (SRL) of the ribosome, which is involved in activation of the GTPase activity of translation factors, such as EF-Tu and EF-G, has been cross-linked to the NTD of RelA (Winther et al., 2018). This observation led to the suggestion that the SRL may be involved in activation of (p)ppGpp synthesis of RelA (Winther et al., 2018). However, we do not observe a stable interaction between the NTD and the SRL, and moreover, α-sarcin, a toxin which cleaves and inactivates the SRL, was reported to have no effect on the ribosome-stimulated (p)ppGpp synthesis of RelA (Kudrin et al., 2018). Taken together, we propose that the (p)ppGpp activity of Rel is activated by adopting an open conformation on the ribosome upon detraction of the inhibitory CTD from the NTD, similar to the mechanism observed for RelA at the SRC.

### Model of Rel Regulation

In conclusion, we propose the following model for the regulation of Rel (Figure 6): in the absence of stress, translating ribosomes are provided with aminoacylated tRNAs (aa-tRNAs) by EF-Tu·aa-tRNA·GTP ternary complexes for protein biosynthesis and Rel resides in a homodimeric Hyd-ON/Syn-OFF state to degrade (p)ppGpp (Figure 6, left). Upon accumulation of deacylated tRNAs (indicative for amino acid starvation), the hypothetical Rel homodimer dissociates to bind deacylated-tRNA for formation of Rel·deacylated-tRNA complexes, which are ''primed' for recruitment to cognate ribosomes (Figure 6, middle). Upon recognition of a cognate ribosome, the preformed Rel·deacylated-tRNA complex associates with the SRC and switches into the Syn-ON and Hyd-OFF state for (p)ppGpp synthesis (Figure 6, right). Because of the close sequence homology and functional similarity of the Gram-negative RelA enzyme, we propose that the activity of RelA might be regulated analogously to the above-described mechanism for the regulation of the Gram-positive Rel protein.

## STAR★METHODS

Detailed methods are provided in the online version of this paper and include the following:

- KEY RESOURCES TABLE
- RESOURCE AVAILABILITY
  - Lead Contact
  - Materials Availability
  - Data and Code Availability

## SUPPLEMENTAL INFORMATION

Supplemental Information can be found online at https://doi.org/10.1016/j.celrep.2020.108157.

## ACKNOWLEDGMENTS

G.B., D.N.W., and K.T. are grateful for financial support from the DFG priority program SPP1879. G.B. and P.P. acknowledge the excellent support by the European Synchrotron Radiation Facility (ESRF), Grenoble, France. We thank Susanne Reider, Otto Berninghausen, and Roland Beckmann (University of Munich, Germany) for help with cryo-EM data collection. We acknowledge the Core Facility of Protein Spectroscopy and Protein Biochemistry of the Philipps-University Marburg. We thank Nils Mais for assistance during the revision of the manuscript.

## AUTHOR CONTRIBUTIONS

P.P. purified proteins, performed the pull-down assays and MALS experiments, and determined the crystal structure. M.A. performed the cryo-EM analysis. W.S. performed the biochemical activity assays. H.S. performed *in vivo* experiments. F.L.G. performed the bacterial 2-hybrid experiment. S.-A.F. and P.P. performed the Bio-layer Interferometry experiments. All authors contributed to the experimental design and analyzed the data. P.P., K.T., D.N.W., and G.B. wrote the manuscript.

## DECLARATION OF INTERESTS

The authors declare that they have no competing interests.

Received: May 12, 2020
Revised: July 10, 2020
Accepted: August 26, 2020
Published: September 15, 2020

## REFERENCES

Adams, P.D., Afonine, P.V., Bunkóczi, G., Chen, V.B., Davis, I.W., Echols, N., Headd, J.J., Hung, L.W., Kapral, G.J., Grosse-Kunstleve, R.W., et al. (2010). PHENIX: a comprehensive Python-based system for macromolecular structure solution. Acta Crystallogr. D Biol. Crystallogr. *66*, 213–221.

Arenz, S., Abdelshahid, M., Sohmen, D., Payoe, R., Starosta, A.L., Berninghausen, O., Hauryliuk, V., Beckmann, R., and Wilson, D.N. (2016). The stringent factor RelA adopts an open conformation on the ribosome to stimulate ppGpp synthesis. Nucleic Acids Res. *44*, 6471–6481.

Arnaud, M., Chastanet, A., and Debarbouille, M. (2004). New Vector for Efficient Allelic Replacement in Naturally Gram-Positive Bacteria. Appl. Environ. Microbiol. *70*, 6887–6891.

Battesti, A., and Bouveret, E. (2012). The bacterial two-hybrid system based on adenylate cyclase reconstitution in Escherichia coli. Methods *58*, 325–334.

Beckert, B., Abdelshahid, M., Schäfer, H., Steinchen, W., Arenz, S., Berninghausen, O., Beckmann, R., Bange, G., Turgay, K., and Wilson, D.N. (2017). Structure of the *Bacillus subtilis* hibernating 100S ribosome reveals the basis for 70S dimerization. EMBO J. *36*, 2061–2072.

Ben-Yehuda, S., Rudner, D.Z., and Losick, R. (2003). RacA, A Bacterial Protein That anchors Chromosomes to The Cell Poles. Science *299*, 532–537.

Biasini, M., Bienert, S., Waterhouse, A., Arnold, K., Studer, G., Schmidt, T., Kiefer, F., Gallo Cassarino, T., Bertoni, M., Bordoli, L., and Schwede, T. (2014). SWISS-MODEL: modelling protein tertiary and quaternary structure using evolutionary information. Nucleic Acids Res. *42*, W252–W258.

Brown, A., Fernández, I.S., Gordiyenko, Y., and Ramakrishnan, V. (2016). Ribosome-dependent activation of stringent control. Nature *534*, 277–280.

Crowe-McAuliffe, C., Graf, M., Huter, P., Takada, H., Abdelshahid, M., Nováček, J., Murina, V., Atkinson, G.C., Hauryliuk, V., and Wilson, D.N. (2018). Structural basis for antibiotic resistance mediated by the *Bacillus subtilis* ABCF ATPase VmlR. Proc. Natl. Acad. Sci. USA *115*, 8978–8983.

Emsley, P., and Cowtan, K. (2004). Coot: model-building tools for molecular graphics. Acta Crystallogr. D Biol. Crystallogr. *60*, 2126–2132.

Gropp, M., Strausz, Y., Gross, M., and Glaser, G. (2001). Regulation of Escherichia coli RelA requires oligomerization of the C-terminal domain. J. Bacteriol. *183*, 570–579.

Haseltine, W.A., and Block, R. (1973). Synthesis of guanosine tetra- and pentaphosphate requires the presence of a codon-specific, uncharged transfer ribonucleic acid in the acceptor site of ribosomes. Proc. Natl. Acad. Sci. USA *70*, 1564–1568.

Haseltine, W.A., Block, R., Gilbert, W., and Weber, K. (1972). MSI and MSII made on ribosome in idling step of protein synthesis. Nature *238*, 381–384.

Hauryliuk, V., Atkinson, G.C., Murakami, K.S., Tenson, T., and Gerdes, K. (2015). Recent functional insights into the role of (p)ppGpp in bacterial physiology. Nat. Rev. Microbiol. *13*, 298–309.

Hogg, T., Mechold, U., Malke, H., Cashel, M., and Hilgenfeld, R. (2004). Conformational antagonism between opposing active sites in a bifunctional RelA/SpoT homolog modulates (p)ppGpp metabolism during the stringent response [corrected]. Cell *117*, 57–68.

Jain, V., Saleem-Batcha, R., China, A., and Chatterji, D. (2006). Molecular dissection of the mycobacterial stringent response protein Rel. Protein Sci. *15*, 1449–1464.

Kabsch, W. (2010). XDS. Acta Crystallogr. D Biol. Crystallogr. *66*, 125–132.

Krissinel, E., and Henrick, K. (2007). Inference of macromolecular assemblies from crystalline state. J. Mol. Biol. *372*, 774–797.

Kudrin, P., Dzhygyr, I., Ishiguro, K., Beljantseva, J., Maksimova, E., Oliveira, S.R.A., Varik, V., Payoe, R., Konevega, A.L., Tenson, T., et al. (2018). The ribosomal A-site finger is crucial for binding and activation of the stringent factor RelA. Nucleic Acids Res. *46*, 1973–1983.

Kushwaha, G.S., Bange, G., and Bhavesh, N.S. (2019). Interaction studies on bacterial stringent response protein RelA with uncharged tRNA provide evidence for its prerequisite complex for ribosome binding. Curr. Genet. *65*, 1173–1184.

Li, N., Chen, Y., Guo, Q., Zhang, Y., Yuan, Y., Ma, C., Deng, H., Lei, J., and Gao, N. (2013). Cryo-EM structures of the late-stage assembly intermediates of the bacterial 50S ribosomal subunit. Nucleic Acids Res. *41*, 7073–7083.

Loveland, A.B., Bah, E., Madireddy, R., Zhang, Y., Brilot, A.F., Grigorieff, N., and Korostelev, A.A. (2016). Ribosome·RelA structures reveal the mechanism of stringent response activation. eLife *5*, e17029.

McCoy, A.J., Grosse-Kunstleve, R.W., Adams, P.D., Winn, M.D., Storoni, L.C., and Read, R.J. (2007). Phaser crystallographic software. J. Appl. Cryst. *40*, 658–674.

Mechold, U., Murphy, H., Brown, L., and Cashel, M. (2002). Intramolecular regulation of the opposing (p)ppGpp catalytic activities of Rel(Seq), the Rel/Spo enzyme from Streptococcus equisimilis. J. Bacteriol. *184*, 2878–2888.

Mehta, P., Woo, P., Venkataraman, K., and Karzai, A.W. (2012). Ribosome purification approaches for studying interactions of regulatory proteins and RNAs with the ribosome. Methods Mol. Biol. *905*, 273–289.

Pettersen, E.F., Goddard, T.D., Huang, C.C., Couch, G.S., Greenblatt, D.M., Meng, E.C., and Ferrin, T.E. (2004). UCSF Chimera—a visualization system for exploratory research and analysis. J. Comput. Chem. *25*, 1605–1612.

Rohou, A., and Grigorieff, N. (2015). CTFFIND4: Fast and accurate defocus estimation from electron micrographs. J. Struct. Biol. *192*, 216–221.

Schäfer, H., Beckert, B., Frese, C.K., Steinchen, W., Nuss, A.M., Beckstette, M., Hantke, I., Driller, K., Sudzinová, P., Krásný, L., et al. (2020). The alarmones (p)ppGpp are part of the heat shock response of Bacillus subtilis. PLoS Genet. *16*, e1008275.

Scheres, S.H. (2012). RELION: implementation of a Bayesian approach to cryo-EM structure determination. J. Struct. Biol. *180*, 519–530.

Singal, B., Balakrishna, A.M., Nartey, W., Manimekalai, M.S.S., Jeyakanthan, J., and Grüber, G. (2017). Crystallographic and solution structure of the N-terminal domain of the Rel protein from Mycobacterium tuberculosis. FEBS Lett. *591*, 2323–2337.

Sohmen, D., Chiba, S., Shimokawa-Chiba, N., Innis, C.A., Berninghausen, O., Beckmann, R., Ito, K., and Wilson, D.N. (2015). Structure of the Bacillus subtilis 70S ribosome reveals the basis for species-specific stalling. Nat. Commun. *6*, 6941.

Spizizen, J. (1958). Transformation Of Biochemically Deficient Strains Of Bacillus Subtilis By Deoxyribonucleate. Proc. Natl. Acad. Sci. USA *44*, 1072–1078.

Steinchen, W., and Bange, G. (2016). The magic dance of the alarmones (p)ppGpp. Mol. Microbiol. *101*, 531–544.

Steinchen, W., Schuhmacher, J.S., Altegoer, F., Fage, C.D., Srinivasan, V., Linne, U., Marahiel, M.A., and Bange, G. (2015). Catalytic mechanism and allosteric regulation of an oligomeric (p)ppGpp synthetase by an alarmone. Proc. Natl. Acad. Sci. USA *112*, 13348–13353.

Stülke, J., Hanschke, R., and Hecker, M. (1993). Temporal activation of beta-glucanase synthesis in Bacillus subtilis is mediated by the GTP pool. J. Gen. Microbiol. *139*, 2041–2045.

Sy, J., and Lipmann, F. (1973). Identification of the synthesis of guanosine tetraphosphate (MS I) as insertion of a pyrophosphoryl group into the 3′-position in guanosine 5′-diphosphate. Proc. Natl. Acad. Sci. USA *70*, 306–309.

Tagami, K., Nanamiya, H., Kazo, Y., Maehashi, M., Suzuki, S., Namba, E., Hoshiya, M., Hanai, R., Tozawa, Y., Morimoto, T., et al. (2012). Expression of a small (p)ppGpp synthetase, YwaC, in the (p)ppGpp(0) mutant of Bacillus subtilis triggers YvyD-dependent dimerization of ribosome. MicrobiologyOpen *1*, 115–134.

Takada, H., Roghanian, M., Murina, V., Dzhygyr, I., Murayama, R., Akanuma, G., Atkinson, G.C., Garcia-Pino, A., and Hauryliuk, V. (2020). The C-Terminal RRM/ACT Domain Is Crucial for Fine-Tuning the Activation of 'Long' RelA-SpoT Homolog Enzymes by Ribosomal Complexes. Front. Microbiol. *11*, 277.

Tamman, H., Van Nerom, K., Takada, H., Vandenberk, N., Scholl, D., Polikanov, Y., Hofkens, J., Talavera, A., Hauryliuk, V., Hendrix, J., and Garcia-Pino, A. (2020). A nucleotide-switch mechanism mediates opposing catalytic activities of Rel enzymes. Nat. Chem. Biol. *16*, 834–840.

Turnbull, K.J., Dzhygyr, I., Lindemose, S., Hauryliuk, V., and Roghanian, M. (2019). Intramolecular Interactions Dominate the Autoregulation of *Escherichia coli* Stringent Factor RelA. Front. Microbiol. *10*, 1966.

Winn, M.D., Ballard, C.C., Cowtan, K.D., Dodson, E.J., Emsley, P., Evans, P.R., Keegan, R.M., Krissinel, E.B., Leslie, A.G., McCoy, A., et al. (2011). Overview of the CCP4 suite and current developments. Acta Crystallogr. D Biol. Crystallogr. *67*, 235–242.

Winther, K.S., Roghanian, M., and Gerdes, K. (2018). Activation of the Stringent Response by Loading of RelA-tRNA Complexes at the Ribosomal A-Site. Mol. Cell *70*, 95–105.e104.

Yang, X., and Ishiguro, E.E. (2001). Dimerization of the RelA protein of Escherichia coli. Biochem. Cell Biol. *79*, 729–736.

## STAR★METHODS

### KEY RESOURCES TABLE

| REAGENT or RESOURCE | SOURCE | IDENTIFIER |
|---|---|---|
| Antibodies | | |
| Rabbit polyclonal Anti-HPF | Beckert et al., 2017 | N/A |
| Bacterial and Virus Strains | | |
| *Escherichia coli* BL21 (DE3) | Novagen | 69449 |
| *Escherichia coli* BTH101 | Euromedex | EUB001 |
| For *B. subtilis* strains see Table S3G (Supplemental Excel table) | N/A | N/A |
| Chemicals, Peptides, and Recombinant Proteins | | |
| Ortho-nitrophenyl-β-galactopyranoside | Thermo Scientific | 34055 |
| ATP (for enzymatic assays) | Jena Bioscience | NU-1010 |
| GTP (for enzymatic assays) | Jena Bioscience | NU-1012 |
| GDP (for enzymatic assays) | Jena Bioscience | NU-1172 |
| Tetrapentylammonium bromide (TPAB) | Thermo Fisher Scientific (ACROS Organics) | AC221481000 |
| 1x Complete EDTA-free Protease Inhibitor cocktail (Roche) | Sigma-Aldrich | 4693132001 |
| RNase H | NEB | M0297 |
| $tRNA^{Lys}$ | Sigma-Aldrich | R6018 |
| GDP (for cryo-EM) | Sigma-Aldrich | G7127 |
| Telithromycin | Santa Cruz Biotechnology Inc. | sc-212994 |
| Alpha, beta-methylene ATP | Sigma-Aldrich | 5.05419 |
| TRIzol | Ambion | 15596018 |
| Critical Commercial Assays | | |
| PURExpress *In Vitro* Protein Synthesis Kit Delta ribosomes | New England BioLabs | E3313 |
| Deposited Data | | |
| Cryo-EM map of *B. subtilis* Rel-ErmDL-RNC complex | This paper | EMDB: EMD-0270 |
| Model of B. *subtilis* Rel-ErmDL-RNC complex | This paper | PDB: 6HTQ |
| X-ray crystal structure of *Bs*Rel 1-556-His | This paper | PDB: 6YXA |
| Oligonucleotides | | |
| For primers used for cloning of heterologous expression constructs see Table S3A (Supplemental Excel table) | N/A | N/A |
| For primers used for cloning of bacterial two-hybrid vectors see Table S3C (Supplemental Excel table) | N/A | N/A |
| For primers used for cloning of *B. subtilis* vectors see Table S3E (Supplemental Excel table) | N/A | N/A |
| For primers used for sequencing of *B. subtilis* vectors and strains see Table S3F (Supplemental Excel table) | N/A | N/A |
| Linker cleavage oligo: 5′-TTCCTCCTTATAAAACT-3′ | Metabion | N/A |
| 2XermDL 5′-TAATACGACTCACTATAGGGAGTT TTATAAGGAGGAAAAAATATGACACA CTCAATGAGACTTAAGTTCCCAACTTTG AACCAGTAAAGTTTTATAAGGAGGAAAA AATATGACACACTCAATGAGACTTAAGTTC CCAACTTTGAACCAGTAA-3′ | Eurofins | N/A |

(*Continued on next page*)

*Continued*

| REAGENT or RESOURCE | SOURCE | IDENTIFIER |
|---|---|---|
| Recombinant DNA | | |
| For heterologous expression vectors see Table S3B (Supplemental Excel table) | N/A | N/A |
| For Bacterial two hybrid vectors see Table S3D (Supplemental Excel table) | N/A | N/A |
| For *B. subtilis* vectors see Table S3H (Supplemental Excel table) | N/A | N/A |
| Software and Algorithms | | |
| Prism 6.0 | Graph Pad | https://www.graphpad.com/scientific-software/prism/ |
| Adobe Illustrator CS6 | Adobe Systems | https://www.adobe.com/products/illustrator.html |
| Agilent ChemStation B.04.01 | Agilent | https://www.agilent.com/store/productDetail.jsp?catalogId=G2070-60121 |
| Gautomatch | https://www.mrc-lmb.cam.ac.uk/kzhang/ | N/A |
| RELION-2 | Scheres, 2012 | N/A |
| CTFFIND4 | Rohou and Grigorieff, 2015 | N/A |
| MotionCor2 | Li et al., 2013 | N/A |
| Chimera | Pettersen et al., 2004 | N/A |
| Coot | Emsley and Cowtan, 2004 | N/A |
| Swiss-modeler | Biasini et al., 2014 | N/A |
| PyMol Molecular Graphic Systems Version 1.8 | Schrödinger (https://www.pymol.org/2/) | N/A |
| XDS | Kabsch, 2010 | http://xds.mpimf-heidelberg.mpg.de/ |
| CCP4 | Winn et al., 2011 | https://www.ccp4.ac.uk/ |
| COOT | Emsley and Cowtan, 2004 | https://www2.mrc-lmb.cam.ac.uk/personal/pemsley/coot/ |
| Phenix suite | Adams et al., 2010 | https://www.phenix-online.org/ |
| Other | | |
| ResourceQ, 6 ml column | Sigma Aldrich | GE17-1179-01 |
| EC 250/4.6 Nucleodur HTec 3 μM | Macherey-Nagel | MN760326.46 |
| HisTrap Fast Flow | GE Healthcare | 17-5319-01 |
| HiLoad 16/600 Superdex 200 column | GE Healthcare | 28-9893-35 |
| Glutathione Sepharose 4B beads | GE Healthcare | 17-0756-01 |
| Superdex 200 Increase 10/300 GL | GE Healthcare | 17-5175-01 |

## RESOURCE AVAILABILITY

### Lead Contact

Further information and requests for resources and reagents should be directed to and will be fulfilled by the Lead Contact, Gert Bange (gert.bange@synmikro.uni-marburg.de).

### Materials Availability

Plasmids and *B. subtilis* strains are available upon request from Gert Bange.

### Data and Code Availability

Cryo-EM map and model have been deposited in the EMDB under accession codes EMD-0270 and PDB under accession code 6HTQ, respectively. Coordinates for the crystal structure of *Bs*RelE have been deposited at the PDB under the accession code 6YXA.

## EXPERIMENTAL MODEL AND SUBJECT DETAILS

*B. subtilis* 168 were grown in synthetic medium (Stülke et al., 1993) supplemented with 0.5% (w/v) casamino acids at 37°C with orbital shaking at 200 rpm or at 37°C over night (18 h) on synthetic medium agar plates. *E. coli* BTH101 were grown on LB agar plates at 37°C and in LB at 30°C overnight, shaking vigorously in a 24-well plate. Strains were stored as glycerol stocks at −80°C.

## METHOD DETAILS

### Cloning, expression, and purification for heterologous production of Rel

*B. subtilis rel* gene fragments were amplified by PCR from *B. subtilis* 168 genomic DNA and cloned into pET24d (Novagen) between the NcoI and BamHI sites to generate expression constructs (see Tables S3A and S3B for primers and plasmids). Mutagenesis of *rel* was performed via overlap extension PCR and subsequent cloning as described above. The *rel*-Hyd-Syn fragment sequence was subcloned from pET24d into pGAT (N-terminal GST) using NcoI and XhoI, or amplified by PCR from full-length mutant genes for cloning into pGAT. Constructs were transformed in *E. coli* BL21(DE3) (Novagen) for overexpression. Cells were inoculated into two liters of LB medium, supplemented with 25 g lactose, ampicillin (100 mg/l) or kanamycin (50 mg/l) depending on the selection marker and incubated at 30°C over night under rigorous shaking (180 revolutions per minute (rpm)). Cells were harvested by centrifugation (3,500 *x g*, 20 min, 4°C) and resuspended in 20 mL lysis buffer (20 mM HEPES-NaOH, pH 8.0, 500 mM NaCl, 40 mM imidazole) before lysis in a M-110L Microfluidizer (Microfluidics). The lysate was cleared at 47,850 *x g* for 20 min at 4°C and the supernatant was applied onto two pre-equilibrated 1 mL HisTrap FF columns (GE Healthcare) for Ni-NTA affinity chromatography. After a wash step with 15 column volumes (CV) of lysis buffer, proteins were eluted with three CV of elution buffer (20 mM HEPES-NaOH, pH 8.0, 500 mM NaCl, 500 mM imidazole). Proteins were concentrated to 1 mL and further purified by size-exclusion chromatography using a HiLoad 16/600 Superdex 200 column (GE Healthcare) equilibrated in size-exclusion buffer (20 mM HEPES-NaOH, pH 7.5, 500 mM NaCl). For the purification of Rel variants used for the enzymatic activity assay, buffers were supplemented with an additional amount of 500 mM NaCl and 5% (v/v) glycerol. The main peak fractions were concentrated and concentrations were determined by measuring the absorbance at 280 nm wavelength using a NanoDrop Lite spectrophotometer. Proteins were flash frozen in liquid nitrogen and stored at −80°C up to two weeks.

### Alarmone preparation, and Rel activity assay

pppGpp was produced as described previously (Steinchen et al., 2015). All Rel-H420E variants were purified as described above. Assays for pppGpp hydrolytic and synthetic activity of Rel were carried out in 20 mM Tris-HCl, pH 7.5, 50 mM NaCl, 1 mM $MnCl_2$ and 10 mM $MgCl_2$. 5 μM of Rel or its variants (see Table S3B) were incubated at 37°C in presence of 1 mM of pppGpp for 10 min (hydrolysis) or 1 mM ATP and 1 mM GTP for 60 min (synthesis). The reactions were stopped by adding two volume parts of chloroform followed by thorough mixing for 15 s, subsequent incubation at 95°C for 15 s and flash-freezing in liquid nitrogen. While thawing, the samples were centrifuged (17,300 *x g*, 30 min, 4°C) and the aqueous phase analyzed by HPLC on an Agilent 1100 Series system (Agilent technologies) equipped with a C18 column (EC 250/4.6 Nucleodur HTec 3 μM; Macherey-Nagel). Nucleotides were eluted isocratically with a buffer containing 50 mM $KH_2PO_4$, 50 mM $K_2HPO_4$, 10 mM TPAB (tetrapentylammonium bromide) and 25% (v/v) acetonitrile and detected at 260 nm wavelength in agreement with standards. pppGpp hydrolytic activity of Rel was estimated by quantification of pppGpp. pppGpp synthetic activity of Rel was estimated by quantification of AMP released equimolar to the alarmone pppGpp during the reaction. All measurements were performed in duplicates.

### Cloning, strain construction, and *B. subtilis* growth assay

*ywaC*$^{E154V}$ and *yjbM*$^{E139V}$ mutations were introduced markerless into *B. subtilis 168* cells by successive transformation and recombination of plasmids pMAD-ywaC$^{E154V}$ and pMAD-yjbM$^{E139V}$ prior to transformation of *rel* constructs (Arnaud et al., 2004; Spizizen, 1958), yielding strain BHS_204. The *rel* gene was amplified from *B. subtilis 168* genomic DNA and cloned into pDR111 (Ben-Yehuda et al., 2003) using the SalI and SphI restriction sites. Mutagenesis of *rel* was performed via overlap extension PCR and subsequent cloning as described above. Rel variants bearing the H77A, D78A or E324V mutation were first cloned in pMAD and subsequently amplified and cloned into pDR111. To generate pDR111-rel$^{H77A\ D78A\ E324V}$, a C-terminal fragment carrying E324V was amplified using primers 44, 63 and used as a megaprimer in a second reaction with primer 42 with rel$^{H77A\ D78A}$ as template. The resulting plasmids (for primers and plasmids see Tables S3E–S3H) were linearized by digestion with ScaI and transformed into naturally competent BHS204 (*ywaC*$^{E154V}$ *yjbM*$^{E139V}$) cells. Transformants were selected on LB agar plates with 100 μg/ml spectinomycin and checked for loss of α-amylase activity. The resulting strains were subsequently transformed with a PCR-amplified fragment encoding *ΔrelA::erm* and selected on LB agar plates containing 1 μg/ml erythromycin, 25 μg/ml lincomycin to generate the ppGpp$^0$ strain background. PCR and DNA sequencing confirmed the identity of the generated plasmids and strains. Strains were grown in synthetic medium (Stülke et al., 1993) supplemented with 0.5% (w/v) casamino acids at 37°C with orbital shaking at 200 rpm. At OD600 of 0.3, the medium was supplemented with 1 mM IPTG. After 30 min, cells were harvested by centrifugation at 3,680 *x g* for 5 min. Cells were resuspended in buffer TE (10 mM Tris-HCl, pH 8.0, 1 mM EDTA) and disrupted by sonication. 8 μg total cleared protein extract was analyzed by SDS-PAGE and western blotting according. Polyclonal antibodies raised against *Bs*HPF (Pineda Antibody Service), *Bs*RelA-NTD (1-387) or rabbit IgG conjugated with HRP (Carl Roth, Karlsruhe, Germany) were used in 5,000-fold dilutions.

Signals were detected using a ChemoStar imaging system (Intas, Göttingen, Germany). For the growth assay on agar plates, stationary-phase cultures were adjusted to an OD600 of 1.0 and serially diluted in 0.9% (w/v) NaCl. 5 μl cell suspension was spotted on LB agar plates with or without 1 mM IPTG. Plates were incubated at 37°C over night (18 h).

### Crystallization, data collection, and structure determination

Purified *Bs*RelΔRIS-CT was concentrated to an absorbance at 280 nm of 20 AU (NanoDrop Lite spectrophotometer), corresponding to an estimated concentration of 22.2 mg/ml, and subjected to crystallization by sitting drop vapor-diffusion at 20°C. Tetragonal bipyramidal crystals grew within one day in drops containing 1 μL *Bs*RelΔRIS-CT and 1 μL crystallization buffer (1 M lithium chloride, 0.1 M bicine pH 9.0, 10% (w/v) PEG6000, final pH 9.0). Crystals were transferred into crystallization buffer containing 20% (v/v) glycerol as cryo-protectant, subsequently flash frozen and stored in liquid nitrogen. Diffraction data was collected at beamline ID29 of the European Synchrotron Radiation Facility (ESRF), Grenoble, France. Data were processed with the XDS program package for data reduction (Kabsch, 2010). Merging and scaling was performed using the AIMLESS program as implemented in the CCP4 package (Winn et al., 2011). The *Bs*RelΔRIS-CT dataset was solved by molecular replacement using the *Sd*Rel-NTD crystal structure (PDB-ID: 1VJ7, chain B; Hogg et al., 2004) via the CCP4-implemented program Phaser (McCoy et al., 2007). Coot (Emsley and Cowtan, 2004) in combination with Refmac5 (CCP4 package) and phenix.refine (PHENIX package) was used for iterative model building and refinement (Adams et al., 2010). Figures were prepared in PyMol (https://pymol.org/2/).

### Bacterial two-hybrid assay

Full-length and truncated versions of *B. subtilis rel* were subcloned from pET24d_His-*Bsrel* into BamHI digested plasmids, pUT18C and pKT25 (Euromedex) by Gibson assembly using oligonucleotides listed in Table S3C. Bacterial two-hybrid experiments were performed as described previously (Battesti and Bouveret, 2012). Briefly, for each interaction experiment, *E. coli* BTH101 (containing a RelA mutation) was co-transformed with two plasmids (pUT18C and pKT25 derivatives) selected on LB agar plates supplemented with 50 μg/ml kanamycin and 100 μg/ml ampicillin. Each interaction measurement is based on analyses of six independently isolated colonies from freshly transformed cells. Clones were inoculated in LB containing 5 mM IPTG and grown at 30°C overnight in a 24-well plate. OD600 was determined and 200 μL of each culture transferred to 800 μL of Z-buffer (8 g of $Na_2HPO_4$ x 12 $H_2O$, 3.125 g of $NaH_2PO_4$ x $H_2O$, 0.375 g of KCl, 0.123 g of $MgSO_4$ x 7 $H_2O$ dissolved in 500 mL distilled water, adjusted to pH 7, 1.35 mL β-mercaptoethanol is freshly added). One drop of 0.01% (m/v) SDS and two drops of chloroform were added and 50 μL of the upper phase transferred to 150 μL of Z-buffer in a 96-well plate. For each sample 40 μL of ortho-nitrophenyl-β-galactosidase (ONPG, 4 mg/ml final concentration) was added and the absorbance at 420 nm wavelength ($A_{420}$) measured in 30 intervals using microtiter plate reader Infinite M200 Pro (Tecan). The relative β-galactosidase activity for each sample was determined by ($A_{420}$ at time t2 - $A_{420}$ at time t1)/ t2 – t1 (sec)/OD600. The time points t2 and t1 were chosen from the linear part of the kinetic.

### Bio-layer Interferometry

The Rel-H420E protein and its truncation variants were purified as described above. All binding steps were performed in 20 mM HEPES-NaOH, pH 7.5, 500 mM NaCl, 200 μM $MnCl_2$ on an Octet K2 System (Pall ForteBio). Ligand proteins were biotinylated using EZ-Link Sulfo-NHS-Biotin (Thermo Scientific #21217 LOT TD261836). The respective protein was incubated with a 2-fold molar excess of EZ-Link for 20 min. Subsequently, the protein was desalted using a Zeba Spin Column (Thermo Scientific #89882 LOT TA262955). The biotinylated proteins were immobilized on Super Streptavidin (SSA) Biosensors (Pall ForteBio) by preparing 200 μl of a 50 μM solution in a black 96-well plate (Greiner) and a loading step for 900 s followed by a washing step for 30 s. The analyte was titrated from 30 μM to 3.75 μM in a 1:1 dilution series in 200 μl final volume. Measurements were repeated at least twice for each of the four concentrations. Association and dissociation were both measured for 600 s (except for ΔRIS-CT both was measured for 900 s). The baseline was recorded prior and after association/dissociation for 120 s in 20 mM HEPES-NaOH, pH 7.5, 500 mM NaCl, 200 μM $MnCl_2$. For each measurement a reference was recorded omitting the analyte in solution. For $K_D$ determination, the reference curves were subtracted from the sample curves. Subsequently, the binding and dissociation curves were fit to standard 1:1, 2:1 or 1:2 global binding models using the Pall ForteBio analysis software (specified in Figure S4B).

### Purification of $tRNA^{Rel}$

Expression constructs were transformed into *E. coli* BL21(DE3) (Novagen) for protein production and purification as described above. The tRNA that was co-purified with Rel ($tRNA^{Rel}$) was extracted using TRIzol (Ambion) according to the manufacturer's protocol.

### GST pull-down assay

50 μL Glutathione Sepharose 4B beads (GE Healthcare) were washed with 1 mL binding buffer (50 mM Tris-HCl, pH 8.0, 500 mM NaCl). The beads were resuspended in 500 μL binding buffer and 4 nmol GST-NTD protein was added for the coupling reaction to the beads for 20 min at 4°C on a turning wheel. Beads were washed twice with 1 mL binding buffer. After discarding of the binding buffer, 1 mL pull down buffer (50 mM Tris-HCl, pH 8.0, 5 mM $MgCl_2$, 100 mM NaCl) was added to the beads. Subsequently, 8 nmol of the TGS-AH fragment and 14 nmol $tRNA^{Rel}$ was added and the beads were incubated for 20 min at 4°C on a turning wheel to allow for complex formation. Beads were washed three times with the respective pull-down buffer and proteins were eluted in 50 μL elution

buffer (20 mM GSH, 50 mM Tris-NaOH, pH 8.0, 500 mM NaCl) for 3 min at 20°C. Finally, beads were pelleted in a tabletop centrifuge at 17,300 *x g* for 3 min at 20°C and 15 μL of the eluate was analyzed on SDS-PAGE (15% (v/v) PAA).

### Analytical size-exclusion chromatography coupled to multi-angle light scattering (SEC-MALS)

Proteins were purified by Ni-NTA and size-exclusion chromatography as described above. 10 nmol protein were injected onto a Superdex 200 Increase 10/300 GL column (GE Healthcare) pre-equilibrated in size-exclusion buffer (20 mM HEPES-NaOH, pH 7.5, 500 mM NaCl, 5% (v/v) glycerol) for analytical size-exclusion chromatography and MALS. MALS-RI experiments were performed with an PN3609 9 angle MALS und a PN3150 RI detector (Postnova, Germany). Due to the co-precipitation of Rel with cellular RNA species during protein purification, which might affect the apparent molecular weight of Rel, we employed the H420E RelΔRIS-CT variants for MALS analysis of proteins.

### Purification of *B. subtilis* 70S ribosomes

*B. subtilis* 70S ribosomes were prepared following a procedure described by Mehta et al. (2012), with some modifications. *B. subtilis 168* cells were grown overnight in LB (Luria-Bertani) liquid medium using baffled flasks at 37°C with shaking (220 rpm). A volume of 6 l of LB medium was inoculated at a 1:100 dilution with an overnight culture and cells were grown to an OD600 of 1.5. Cells were harvested by centrifugation at 5,000 × *g* for 15 min at 4°C (Sorvall, SLC 6000 rotor) and the cell pellet was resuspended in buffer A (20 mM HEPES-KOH, pH 7.4, 30 mM $NH_4Cl$, 10 mM $Mg(OAc)_2$, 6 mM β-mercaptoethanol and 1x Complete EDTA-free Protease Inhibitor cocktail (Roche)). Cells were then disrupted using the microfluidizer M110-L (Microfluidics), followed by centrifugation at 30,000 × *g* for 30 min at 4°C to remove cellular debris (Sorvall, SS-34 rotor). The supernatant was then centrifuged at 151,457 × g (Type 45 Ti, Beckman Coulter) for 4.5 h at 4°C. The crude ribosome pellet was resuspended in 5 mL of cold buffer A and loaded onto a 10%–50% (w/v) sucrose gradient (total of 100 $A_{260}$/ml per tube) followed by centrifugation at 89,454 × *g* using an SW28 rotor (Beckman Coulter) for 4 h at 4°C. The fractions corresponding to the 70S ribosomes were collected using a Gradient Station (Biocomp) with an Econo UV Monitor (Biorad) and a FC203B Fraction Collector (Gilson). The collected fractions were then pooled together and the 70S ribosomes pelleted at 92,159 × *g* for 2.5 h at 4°C using a TLA-110 rotor (Beckman Coulter). The 70S pellet was re-suspended in buffer A followed by concentration determination and then aliquots were snap-frozen in liquid nitrogen and stored at −80°C.

### Generation and purification of the *B. subtilis* SRC

The *B. subtilis* stalled ribosome complex (SRC) was generated based on the disome approach similar to that used previously for the *E. coli* RelA·SRC (Arenz et al., 2016; Figure S5). However, the *2XermCL* construct used for the *E. coli* RelA·SRC did not work efficiently with *B. subtilis* ribosomes (data not shown) and was therefore replaced by a construct based on the ErmDL leader peptide (Uniprot-ID: P62188) derived from the macrolide resistance plasmid pE194. The *ermDL* sequences used in the *2XermDL* construct were modified from the original sequence by substitution of the 8$^{th}$ codon CGT (Arg) with AAG (Lys). The *2XermDL* construct was then synthesized (Eurofins, Germany) such that it contained a T7 promoter followed by a strong ribosome binding site (RBS) spaced by seven nucleotides to the ATG (AUG start codon) of the first *ermDL_R8K* cistron. A linker of 22 nts separated the stop codon of the first *ermDL_R8K* cistron and the start codon of the second *ermDL_R8K* cistron. The linker also comprised the strong RBS seven nucleotides upstream of the ATG start codon of the second *ermDL_R8K* cistron, enabling initiation of translation independent from the first *ermDL_R8K* cistron. The complete sequence of *2XermDL_R8K* construct is: 5′-*TAATACGACTCACTATAGGG*AGTTTTATAA**GGAGG**AAAAAATATGACACACTCAATGAGA**CTT**AAGTTCCCAACTTTGAACCAGTAAAGTTTTATAA**GGAGG**AAAAAATATGACACACTCAATGAGA**CTT**AAGTTCCCAACTTTGAACCAGTAA-3′ (T7 promoter, italics; RBS, bold; ErmDL ORF, underlined with CTT codon in P-site of stalled ribosome shown in bold; annealing site for complementary DNA oligonucleotide, underlined). *In vitro* translation of the *ermDL_R8K* construct was performed using 12 μg of *ermDL_R8K* PCR product, 100 μM telithromycin dissolved in DMSO (0.3% (v/v) final DMSO concentration) as well as 600 pmoles of purified *B. subtilis* 70S ribosomes in 250 μL reaction of the PURExpress delta ribosome kit (NEB). Translation reactions were analyzed on sucrose density gradients (10%–55% (w/v) sucrose in buffer A (50 mM HEPES-KOH, pH 7.4, 100 mM KOAc, 25 mM $Mg(OAc)_2$, 6 mM β-mercaptoethanol, 100 μM telithromycin and 1x Complete EDTA-free Protease Inhibitor cocktail (Roche)) by centrifugation at 154,693 × *g* (SW40 rotor, Beckman Coulter) for 3 h at 4°C. For ErmDL_R8K·70S complex purification, disome fractions were collected using a Gradient Station (Biocomp) with an Econo UV Monitor (Biorad) and a FC203B Fraction Collector (Gilson). Purified ErmDL_R8K disomes were concentrated by centrifugation at 88,760 × *g* for 4 h at 4°C (TLA120.2 rotor, Beckman Coulter). To obtain monosomes of the ErmDL_R8K·70S complex, a short DNA oligonucleotide (5′-ttcctccttataaaact-3′, Metabion) was annealed to the linker between the *ermDL_R8K* cistrons, generating a DNA-RNA hybrid that could be cleaved by RNase H (NEB) treatment in buffer A at 25°C for 1 h. After cleavage of the disomes, ErmDL_R8K·70S complex monosomes were again purified and concentrated by centrifugation at 88,760 × *g* for 4 h at 4°C (TLA120.2 rotor, Beckman Coulter).

### Generation of the *B. subtilis* Rel·SRC

The *B. subtilis* Rel·SRC was assembled similarly to that used previously for the *E. coli* RelA·SRC (Arenz et al., 2016; Figure S5). The *B. subtilis* Rel·SRC was formed using a final concentration of 0.125 μM ErmDL_R8K·70S complex monosomes, 0.625 μM *B. subtilis*

Rel (N-terminal $His_6$-tag), 0.625 μM $tRNA^{Lys}$ (Sigma-Aldrich), 500 μM α, β-methylene-ATP (Sigma-Aldrich), 500 μM GDP and 10 μM telithromycin. All components were pre-dissolved in buffer A and the reaction was incubated at 37°C for 20 min.

### Cryo-electron microscopy and single particle reconstruction

A total of 5 $A_{260}$/ml of the *B. subtilis* Rel·SRC was applied to 2 nm pre-coated Quantifoil R3/3 holey carbon supported grids and vitrified using a Vitrobot Mark IV (FEI, Netherlands). Data collection was performed using EM-TOOLS (TVIPS GmbH) on a Titan Krios transmission electron microscope equipped with a Falcon II direct electron detector (FEI) at 300 kV at a pixel size of 1.084 Å and a defocus range of 0.7-2.2 μm. Ten frames (dose per frame of 2.4 $e^-/Å^2$) were aligned using Motion Correction software (Li et al., 2013). Power-spectra, defocus values and astigmatism were determined with CTFIND4 software (Rohou and Grigorieff, 2015). Micrographs showing Thon rings beyond 4 Å were manually inspected for good areas and power-spectra quality. Automatic particle picking was performed on 4,411 micrographs using Gautomatch (https://www.mrc-lmb.cam.ac.uk/kzhang/) and *E. coli* 70S as a template (Arenz et al., 2016). 2-dimensional class averaging was performed to exclude non-ribosomal particles and then single particles were processed using RELION 2.1 (Scheres, 2012). 650,054 particles were first subjected to 3D refinement using the *B. subtilis* 70S ribosome as reference structure (Sohmen et al., 2015). This was followed by 3D classification using RELION into 10 classes with 6 distinct subpopulations (Figure S5F). Only subpopulation 1 (67,047 particles) had stoichiometric density for Rel and was further refined to yield a final reconstruction with an average resolution (at 0.143 FSC) of 4.5 Å (Figure S6A) with local resolution reaching to 3.8 Å (Figures S6B and S6C) within the core of the ribosomal subunits. The other subpopulations 2-6 did not contain density for Rel, but rather had various combinations of A-, P- and E-site tRNAs.

### Molecular model of the *B. subtilis* Rel·SRC

Homology models of the *B. subtilis* Rel TGS, RIS and ACT subdomains were generated using Swiss-model (Biasini et al., 2014) and could be unambiguously rigid body-fitted using UCSF Chimera (Pettersen et al., 2004) into the electron density of the cryo-EM map of the *B. subtilis* Rel·SRC (Figures S6D–S6I). The homology model for the TGS, ACT, and RIS subdomains of *B. subtilis* Rel were based on *E. coli* RelA·70S complex (PDB-ID 5IQR; Brown et al., 2016). TGS (residues 390-469), RIS (residues 585-655) and ACT (residues 656-731) correlated with *E. coli* template model residues 404-505, 594-662, 663-744 respectively. In order to yield the best fit, each domain was fitted individually as a rigid body into the locally filtered density of the *B. subtilis* Rel·SRC (Figures S6D–S6I). The homology model for the AH subdomain of *B. subtilis* Rel was based on the AH subdomain from the *E. coli* RelA in the *E. coli* RelA·70S complex (PDB-ID: 5KPX; Loveland et al., 2016; Figure S6H). The models for A/R-tRNA, P-tRNA and E-tRNA were taken from the *E. coli* RelA·70S complex (PDB-ID: 5IQR; Brown et al., 2016) and also fitted as rigid-bodies into the cryo-EM map of the *B. subtilis* Rel·SRC complex (Figure S6E). The models for the *B. subtilis* ribosomal subunits were based on the PDB-IDs 3J9W and 6HA1 (Crowe-McAuliffe et al., 2018; Sohmen et al., 2015).

## QUANTIFICATION AND STATISTICAL ANALYSIS

For the Rel activity assay, nucleotide concentrations were quantified using the Agilent ChemStation B.04.01 (Agilent) software and data was analyzed using Prism 6.0 (Graphpad). The statistical details for all experiments can be found in the figure legends and STAR Methods section. Quantification, statistical analysis, and validation for the X-ray crystal structure determination and cryo-EM 3D reconstruction are implemented in the software packages used for data processing and model refinement.